05
-28-81

SERI/TR-8002-7-T2
(DE81025647)

DEVELOPMENT OF PHOTOELECTROCHEMICAL CELLS BASED ON COMPOUND SEMICONDUCTORS AND NONAQUEOUS ELECTROLYTES

Final Report for the Period May 1, 1979—April 30, 1980

By
R. D. Rauh
R. H. Micheels
P. A. Hoenig
M. E. Langmuir
M. A. Parker
D. R. Pratt

D15t-225
pT13-25

October 1980

Work Performed Under Contract No. AC02-77CH00178

EIC Laboratories, Inc.
Newton, Massachusetts

MASTER

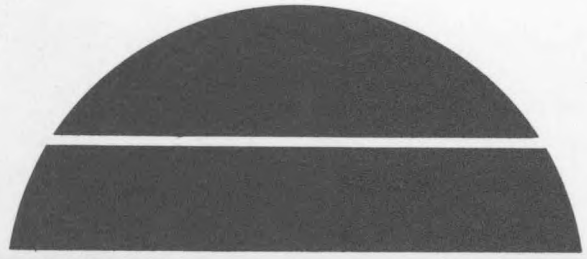

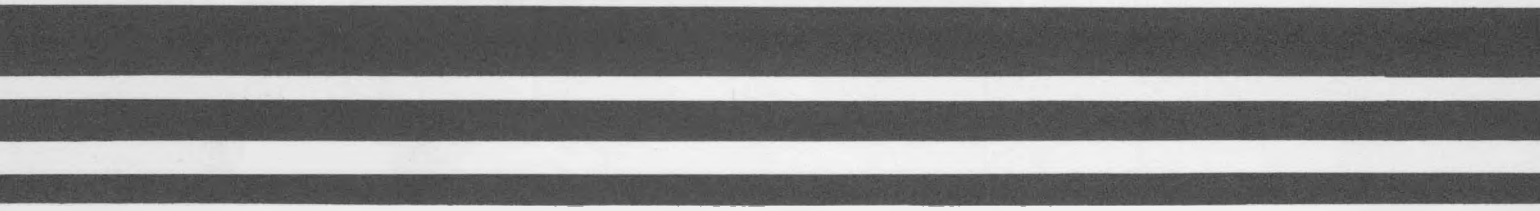

U.S. Department of Energy

Solar Energy

DISCLAIMER

This report was prepared as an account of work sponsored by an agency of the United States Government. Neither the United States Government nor any agency thereof, nor any of their employees, makes any warranty, express or implied, or assumes any legal liability or responsibility for the accuracy, completeness, or usefulness of any information, apparatus, product, or process disclosed, or represents that its use would not infringe privately owned rights. Reference herein to any specific commercial product, process, or service by trade name, trademark, manufacturer, or otherwise does not necessarily constitute or imply its endorsement, recommendation, or favoring by the United States Government or any agency thereof. The views and opinions of authors expressed herein do not necessarily state or reflect those of the United States Government or any agency thereof.

DISCLAIMER

Portions of this document may be illegible in electronic image products. Images are produced from the best available original document.

SERI/TR-8002-7-T2
(DE81025647)
Distribution Category UC-61c

DEVELOPMENT OF PHOTOELECTROCHEMICAL CELLS BASED ON COMPOUND SEMICONDUCTORS AND NONAQUEOUS ELECTROLYTES

Final Report
May 1, 1979 to April 30, 1980

R. D. Rauh, Principal Investigator
M. E. Langmuir, Program Manager
R. H. Micheels, Senior Scientist
M. A. Parker, Staff Scientist
P. A. Hoenig, Staff Scientist
D. R. Pratt, Staff Scientist

EIC Laboratories, Inc.
55 Chapel Street
Newton, Massachusetts 02158

October, 1980

Prepared for the
SOLAR ENERGY RESEARCH INSTITUTE
Under Subcontract No. XP-9-8002-7
Under
Prime Contract No. EG-77-C-01-4042

ABSTRACT

Factors limiting the performance of nonaqueous EPCs have been delineated for a model photoelectrode, n-GaAs, in a variety of solvent-electrolyte combinations. Although a wider range of stabilizing redox systems can be identified in nonaqueous solvents than in H_2O, the lack of specific adsorption of the redox systems still limits maximum open circuit voltages to <0.7V. Because of solubility and conductivity limitations, nonaqueous solvents also present special problems of mass transport and resistive limitations. To date, the best compromise of electrode stability, redox solubility and electrolyte conductivity is found to be the CH_3CN, I_3^-/I^- system for n-GaAs. EPCs using this electrolyte have been characterized in detail. Development of less optically dense electrolytes is also being pursued. Truly anhydrous solutions of Cu and Cr perchlorates have been formed by in situ anodic dissolution of the parent metals.

A parallel study of thin film photoelectrode structures has been conducted to demonstrate nonvacuum deposition methods: screen printing, electroless chemical plating, and electrochemical plating of Cd chalcogenides.

TABLE OF CONTENTS

LIST OF FIGURES

LIST OF FIGURES
(Continued)

LIST OF TABLES

LIST OF TABLES
(Continued)

I. THE PHOTOELECTROLYSIS PROBLEM

As with all solar cells, the goal of EPC research is to produce cells of high efficiency through optimization of photovoltage (V), photocurrent (i_p) and fill factor. As shown in Figure 1, the i-V characteristics of an EPC is a composite of the half cell i-V curves for the individual electrodes. In a simple cell, these would be the active, light absorbing photoelectrodes and a metallic counter electrode. These half-cell i-V curves are further modified by the iR drop within the electrolyte, which acts as a series resistance. The open circuit voltage of the cell (V_{oc}) is the separation between the onsets of counter and photoelectrode currents. Similarly, the short circuit current, i_{sc}, is found at that singular voltage where currents at the two electrodes are equal. Intermediate points on the full cell i-V curve are obtained by finding the polarization of each electrode corresponding to a given current, and subtracting the sum of these polarization voltages from V_{oc}.

We will first ask: what are the limits to the photovoltage in such a cell? In the ideal case, the counter electrode senses the rest potential of the solution, and is thus equivalent to V_{redox}. The photoelectrode has a maximum onset voltage corresponding to its flat band potential, V_{fb}, leading to the relation

$$V_{oc}(max) = V_{fb} - V_{redox} \qquad (1)$$

This simple relation is fundamental to EPC operation, but remains essentially untested in the literature. The relation is also meaningless if the redox couple in the cell is not oxidized or reduced by the photoelectrode so as to stabilize it against photocorrosion. Thus, we further specify the photovoltage by

$$V_{oc}(max) = V_{fb} - V_c \qquad (2)$$

where V_c is the anodic or cathodic corrosion potential of the photoanode or photocathode, respectively. One of the potential advantages of nonaqueous solvents is to allow the maximization of (1) through the maximization of (2) assuming that corrosion reactions are rendered more difficult than in H_2O.

Two factors appear to complicate the use of equation (1) as a simple prediction for cell design. The first is that V_{fb} is influenced by the redox couple when specific adsorption occurs. For example, in the aqueous-based CdX/X_n^{-2}, X^{-2} cells (X = S, Se, Te), V_{fb} is shifted negative by such adsorption (1). The only documented cases of this kind of influence on V_{fb} occur in protic media due to acid-base equilibria involving surface

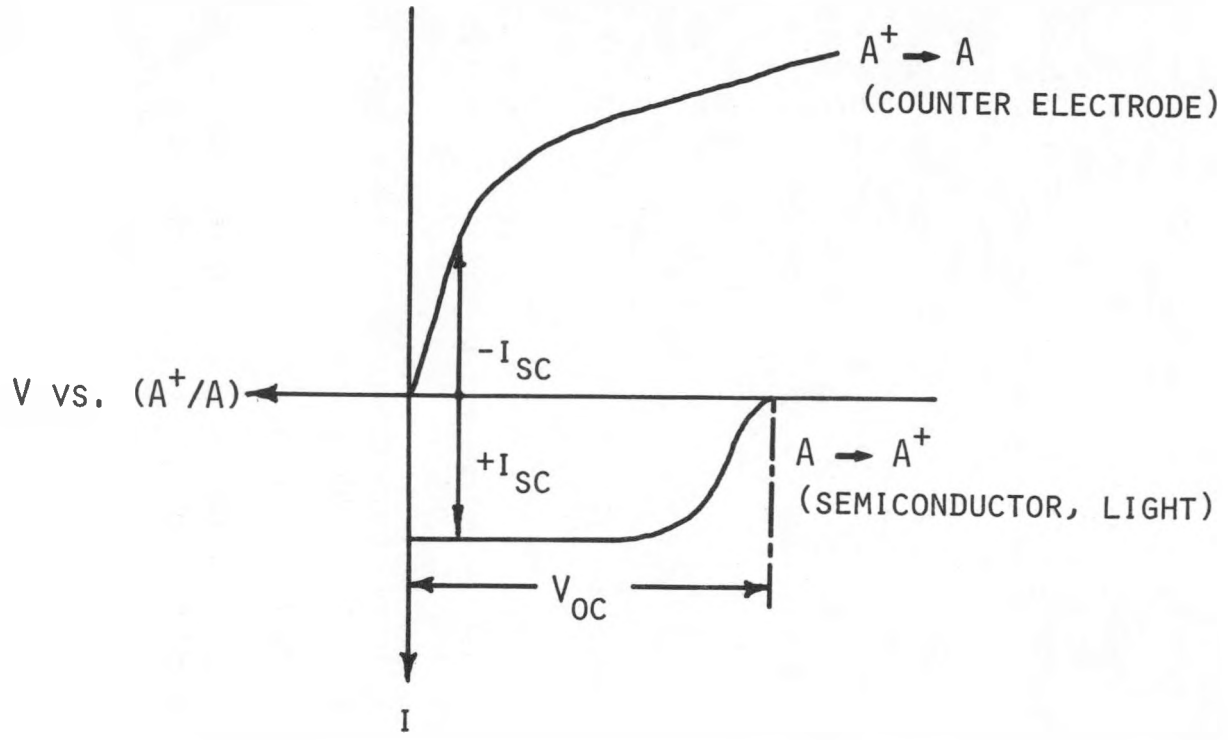

Fig. 1. Steady state current-voltage curves for half-cell components of an electrochemical photovoltaic cell.

OH or XH groups. Thus, we might be able to test equation (1) in aprotic media without this additional variable.

The other complicating factor involves the observation that half cell photovoltages equivalent to V_{fb} are often unattainable. In solid state Schottky barrier devices, this is often ascribed to the intermediacy of "surface states" (2). The latter may be viewed as surface-bound redox centers which act as very efficient captors of electrons or holes. As a result, such centers "pin" the Fermi level, thus restricting the photovoltage. It may be possible to modify, chemically, such states. Improvements in cell operation due to certain semiconductor etching treatment, oxidation, hydrogenation, or treatment with Ru^{+3} have been ascribed to such surface state modification (3-6). Recent observations by Wrighton, Bard and co-workers confirm Fermi level pinning in some EPC devices (7).

The other major question regarding cell operation concerns the factors which influence the photocurrent. The effects on photocurrent yields of redox potential, interaction of the electrolyte with the electrode surface, surface states, and the doping, orientation and crystalline quality of the photoelectrode are little understood. "Surface states" can, for example, influence the voltage onset and rise of photocurrent. Recombination via the surface has been used to explain the so-called "foot problem" in EPC i-V curves, characteristic of inefficient electrodes with low fill factor (3,8). We anticipate that the following factors influence photocurrent yields in EPC devices:

1. Crystal quality and doping level of the photoelectrode insofar as they determine the diffusion length of photogenerated minority carriers.

2. The conductivity of the electrolyte and the resistive losses native to the cell geometry.

3. The concentration of redox species.

4. The density of surface states acting as electron-hole recombination centers.

5. The energetic overlap between semiconductor and redox density of states functions.

6. Specific adsorption of the redox species on the photoelectrode surface.

7. The kinetics of the electron transfer reaction, at both electrodes.

8. Shunt losses via dark electrochemical processes at the photoelectrode caused by tunneling through the space charge layer.

In the first part of this research year, we have employed single crystal GaAs electrodes, and have focused on documenting factors 4-8. The second year will focus more on economical electrodes and cell design, and thus will center on 1-3.

In our view, electrolyte development is one of the most crucial aspects of EPCs. The specific conductances of a number of nonaqueous electrolytes are presented in Table 1. The best of these have specific conductivities of $\sim 0.05\ \Omega^{-1}\text{-cm}^{-1}$. For a typical solar cell, a minimum current of 10 mA/cm^2 must be carried with a maximum voltage loss of 0.1V. Thus, the effective cell thickness must not exceed 0.5 cm, in the most favorable case. It is unlikely that THF and 1,2 DME would meet these criteria using conventional electrolyte salts, although their low dielectric constants may give rise to high photoelectrode stability. Best first choices of the common aprotic solvents appear to be acetonitrile, acetone, and dimethyl formamide, with propylene carbonate being marginal. On the basis of conductivities alone, alcohols appear to hold little advantage over aprotic solvents, and have rather narrow electrochemical windows by comparison.

The other issue is the redox couple. If the Fermi level is pinned by surface states, the voltage attainable will be independent of V_{redox} (7), so that any redox couple which does not decompose the semiconductor may be useful. The variation of photovoltage with V_{redox} is a critical issue addressed during Phase I of the research. In our opinion, the best redox electrolytes will be composed of simple inorganics, metal ions, or photochemically stable metal ion complexes. Soluble salts or complexes of transition ions which have two stable oxidation states are particularly desirable, e.g., Mn(II)/Mn(III), Cr(II)/Cr(III), Fe(II)/Fe(III), Cu(I)/Cu(II) and Co(II)/Co(III). In general, ionic complexes must have bulky counter ions to avoid precipitation in aprotic solvents, e.g., $(Alk_4N)_3Fe(CN)_6$. Similar highly soluble salts of transition metal ions which may be unstable in the solid state can be prepared <u>in situ</u> by electrochemical dissolution of the parent metal.

TABLE 1

SPECIFIC CONDUCTIVITIES OF SOME NONAQUEOUS ELECTROLYTE SOLUTIONS

Solvent	Solute	Concentration of Solute	Specific Conductivity ($\times 10^3\ \Omega^{-1}\ cm^{-1}$)
Acetonitrile	Et_4NClO_4	0.60	38
	Et_4NBF_4	1.0	56
	Bu_4NClO_4	0.6	27
1,2 Dimethoxy Ethane	Bu_4NBF_4	1.0	4.4
	Bu_4NClO_4	1.0	3.2
	KPF_6	1.2	6.2
	$LiClO_4$	0.5	3.22
DMF	Et_4NClO_4	0.60	19.2
	Et_4NBF_4	1.0	26.3
	Bu_4NBF_4	1.0	14.5
	Bu_4NClO_4	0.60	13.0
	KPF_6	1.22*	25.2
	$LiClO_4$	1.16*	22.2
DMSO	$LiClO_4$	1.5*	10
Methyl Formate	$LiClO_4$	2.8*	32
N-Methylpyrrolidone	KPF_6	0.92*	9.4
	$LiClO_4$	0.85*	11.2
PC	KPF_6	1.0*	8
H_2O	KCl	1.0	111
Dioxolane	$LiClO_4$	1.5	20

*Concentration giving maximum conductivity.

II. BASIC MECHANISMS IN ELECTROCHEMICAL PHOTOVOLTAIC CELLS: n-GaAs/PROPYLENE CARBONATE

A. General Approach

The overall aim of this program is to develop an EPC with optimal figures of merit based on nonaqueous electrolytes. The latter are meant to impart long-term stability of the photoelectrode during cell operation. Part of the first year of research was designed to provide an understanding of the factors which determine the open circuit voltage, short circuit current, fill factor and stability of such systems. The model system employed for this study was n-GaAs in contact with a propylene carbonate (PC) based redox electrolyte. Propylene carbonate was chosen for its wide anodic and cathodic stability range, and because we have established procedures for its effective drying and purification. In addition, PC supports a stable Li^+/Li reference electrode which is simple to use and which can be employed without danger of solution contamination. We note later, however, that the low conductivity of PC electrolytes probably prevents its use in practical devices. Nevertheless, the aspects of photoelectrochemical operation discovered in PC can be generalized to other nonaqueous systems.

B. Experimental Methods

Experimental details have been presented in previous reports and need only be summarized here. Most research has been carried out in a demountable thin layer photoelectrochemical research cell shown in Figure 2. The cell has a liquid path length of $\sim$0.4 mm. Irradiation occurs through an optically transparent electrode of tin oxide (NESA) or indium-tin oxide (NESATRON). The electrodes are mounted in a Macor machinable glass block. Filling is carried out in the glove box (<10 ppm H_2O, Ar atmosphere) through the holes containing the demountable Pt electrodes. The photoelectrode is sealed into the block using an epoxy cement previously tested for solvent compatibility. All the desired electrochemical and photoelectrochemical measurements can be made in this cell, as shown in the figure. One of the Pt electrodes serves as a reference electrode, placing V_{redox} at 0 volts in each cell.

The supporting electrolytes in our cells have been Li salts, particularly $LiAsF_6$ and $LiClO_4$. This allows us to calibrate the internal reference electrode vs. Li^+/Li (in a separate measurement), at least for those solvents showing Li compatibility. The Li^+/Li potential is known versus aqueous SCE in a variety of nonaqueous solvents. The liquid-junction corrected value of $E°(Li^+/Li)$ are -2.94V vs. $(SCE)_{aq}$ in PC (12) and -3.17V vs. $(SCE)_{aq}$ in ACN (13). The potentials of some of the specific redox solutions in PC which we have employed are listed in Table 2.

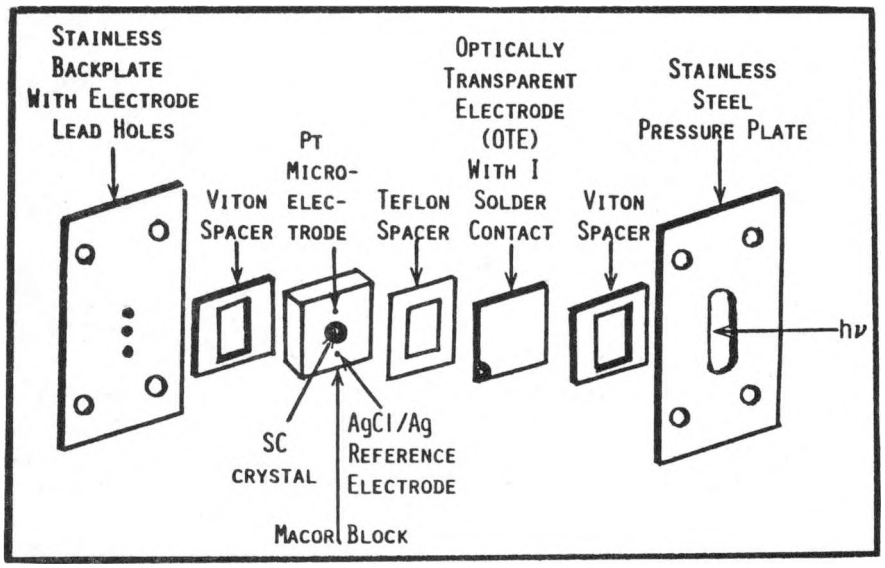

Fig. 2. Demountable thin layer photoelectrochemical research cell.

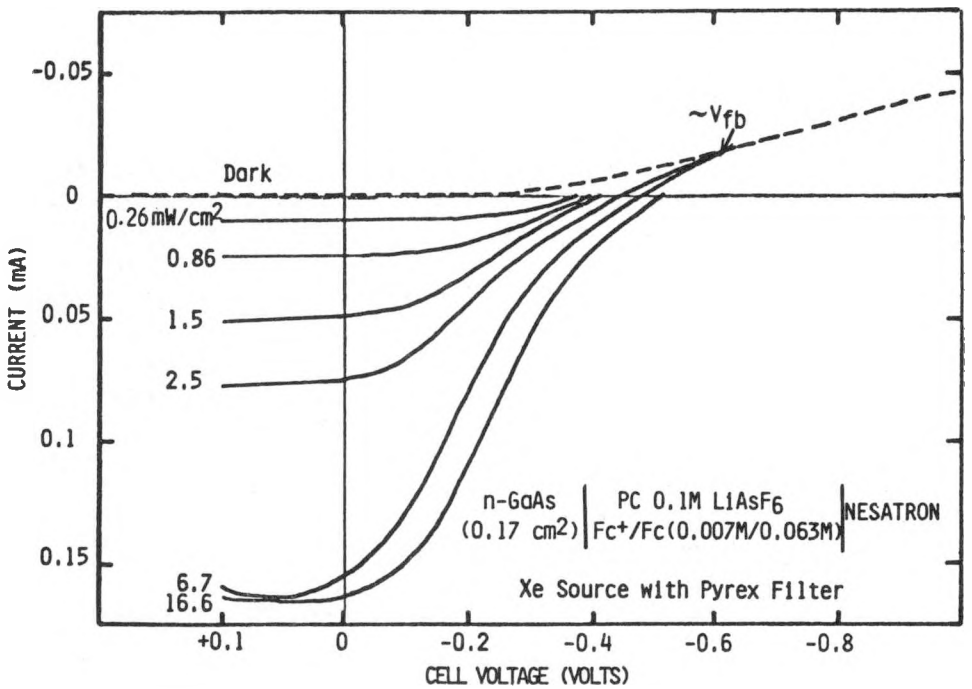

Fig. 3. Current vs. voltage for a n-GaAs EPC as a function of light intensity.

TABLE 2

MEASURED REDOX POTENTIALS FOR COUPLES
IN PROPYLENE CARBONATE

Couple		V_{meas} (vs. SCE_{aq})*
Br_2/Br^-	(0.01M/0.05M)	+0.96
$acFc^+/acFc$	(0.007M/0.03M)	+0.59
Fc^+/Fc	(0.007M/0.063M)	+0.34
I_2/I^-	(0.01M/0.05M)	+0.16
$TMPD^+/TMPD$	(0.01M/0.09M)	-0.01
Li^+/Li		-2.94

acFc: acetyl ferrocene
Fc: ferrocene
TMPD: tetramethyl phenylenediamine

*Liquid junction corrected values.

C. Factors Influencing the Photovoltage

Electrodes were n-GaAs with a <100> orientation, 0.11 Ω-cm Si doped and partially Zn compensated. A typical series of current-voltage curves are shown in Figure 3 for the cell:

$$\text{n-GaAs} \left| \begin{matrix} \text{PC, 0.1M } LiAsF_6 \\ Fc^+/Fc \text{ (0.007/0.063M)} \end{matrix} \right| \begin{matrix} \text{Optically} \\ \text{Transparent Electrode} \end{matrix}$$

In this cell, which contains a rather dilute redox electrolyte, the mechanisms of current and voltage control are evident. In the dark, no anodic current flows. However, a dark cathodic current is observed with an onset of -0.2V*. The magnitude of this current is proportional to the concentration of oxidized species. Its onset is considerably positive of the flat band potential of n-GaAs.

The positive onset of dark current is indicative of a process involving the tunneling of electrons from the conduction band through the space charge region. We have investigated this as a function of the redox potential of the species in solution (V_{redox}). In Figure 4, the

*Electrochemical measurements were made in both 2 and 3 electrode configurations. For the cell featured in Figure 3, the counter electrode has been shown to be much more polarizable than the n-GaAs, and has a negligible contribution to the total cell polarization at the current levels employed. In other systems where the redox reactions have kinetic limitations, such as in I_3^-/I^- cells, this is not always the case.

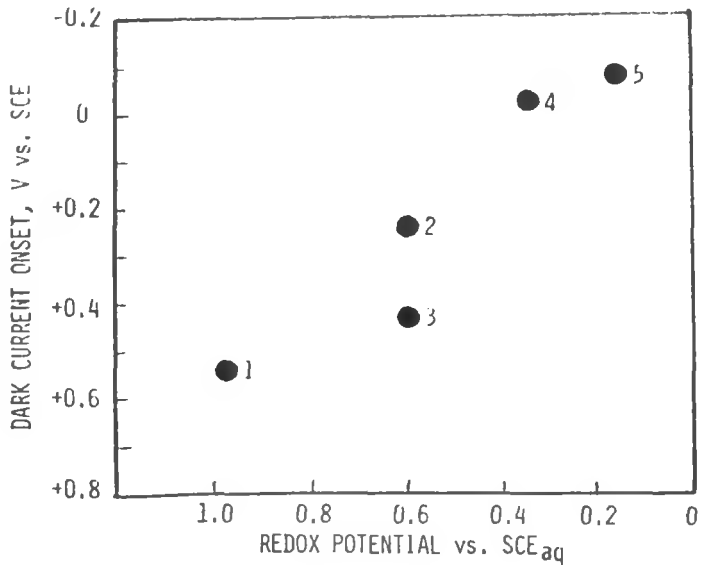

Fig. 4. Dark current onset vs. redox potential for the cell

$$\text{n-GaAs} \left| \begin{array}{c} \text{[ox]/[red]} \\ \text{0.1M LiAsF}_6\text{, PC} \end{array} \right| \text{NESA}$$

Numbers refer to the following redox couples with molar concentrations in parenthesis:

1 - Br_2/Br^- (0.01/0.05)
2 - I_2/I^- (0.05/0.01)
3 - $acFc^+/acFc$ (0.007/0.03)
4 - Fc^+/Fc (0.007/0.063)
5 - I_2/I^- (0.01/0.05)

voltage onset of dark current (V_{dark}) is plotted vs. V_{redox}, both on the aqueous SCE scale. In the region from 0 to +1 vs. SCE, V_{dark} is directly proportional to V_{redox}. This result would be consistent with a surface state controlled barrier potential, which would render $V_{fb}-V_{redox}$ independent of V_{redox}. It is also possible that the dark reaction occurs through a continuum of interface states, so that its onset potential is a function only of V_{redox}.

Returning to Figure 3, we see next that, on irradiation, an anodic photocurrent is produced. The onset of photocurrent at each intensity corresponds to the open circuit voltage, V_{oc}. It occurs at the voltage where dark and photocurrents are exactly equal. Thus, the dark current-voltage behavior of the photoelectrode is important in determining the open circuit voltage of the cell. If V_{dark} always occurred at the same potential, we might hope to adjust V_{redox} to minimize the dark current effect. This is, however, not the case, as seen in Figure 4.

Even though a dark current always opposes the photocurrent, regardless of V_{redox}, cells with large separations between V_{redox} and the apparent flat band voltage, V_{fb}, still have larger open circuit voltages. In Figure 5, the open circuit photovoltages of these cells are plotted vs. V_{redox}. The measurements were made at a high light intensity, where the photovoltage exhibits saturation. For the couples studied, the variation of V_{oc} is quite linear with V_{redox}. Other experiments with variable light intensity have demonstrated that, at low light intensity, photovoltages tend to extrapolate to ∿0.2V. This corresponds to the onset of dark current in each case on the internal scale. The variation of photovoltage with light intensity is therefore greater with more positive V_{redox}. The slopes of the linear portions of the photovoltage-intensity curves, dF/d(log I), are presented in Table 3.

TABLE 3

VARIATIONS OF PHOTOVOLTAGE WITH LIGHT INTENSITY FOR THE CELL

n-GaAs|PC, redox, 0.1M $LiAsF_6$|NESA

Solution		V_{redox} (meas)	dV/d(log I) (mV)
Br_2/Br^-	(0.01/0.05M)	0.96	50
$acFc^+/acFc$	(0.007/0.03M)	0.59	170
Fc^+/Fc	(0.007/0.063M)	0.34	125
I_2/I^-	(0.01/0.05M)	0.16	88
$TMPD^+/TMPD$	(0.01/0.09M)	-0.01	55

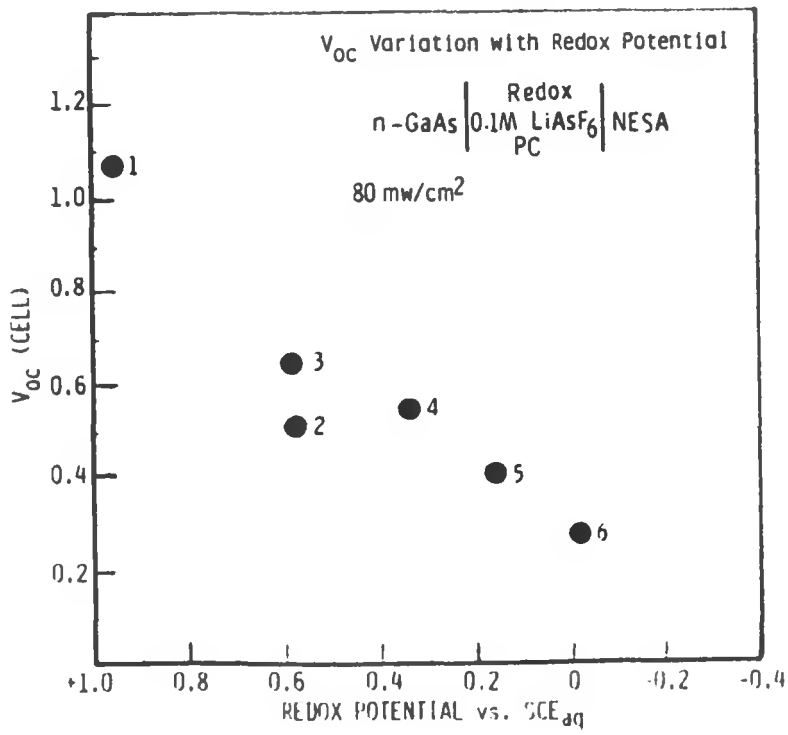

Fig. 5. Variation of V_{OC} with solution redox potential for n-GaAs EPC.

1 -	Br_2/Br^-	(0.01/0.05M)
2 -	I_2/I^-	(0.05/0.01M)
3 -	$acFc^+/acFc$	(0.007/0.03M)
4 -	Fc^+/Fc	(0.007/0.063M)
5 -	I_2/I^-	(0.01/0.05M)
6 -	$TMPD^+/TMPD$	(0.01/0.09M)

An important point concerning photovoltages in photoelectrochemical cells is illustrated by the case of the Br_2/Br^- couple, which is an exception to the above discussion. In these cells, GaAs appears to corrode according to the reaction

$$2GaAs + 3Br_2 \rightarrow 2Ga^{+3} + 6Br^- \qquad (3)$$

Hence, the redox couple is ineffective in stabilizing the semiconductor.* In these cases, the open circuit voltage of the cell is given by the difference $V_{redox}-V_{corrosion}$. This difference can be made large by choosing any redox couple, but the resulting photovoltages are meaningless unless it is established that the redox couple is indeed photoelectrochemically oxidized or reduced.

In Figure 6, V_{oc}, V_{redox} and V_{dark} are summarized for the redox couples studied, with all potentials presented on the aqueous SCE scale. It is seen that V_{oc} under high light intensities is about -0.2V for the n-GaAs half cell regardless of the redox couple in solution. This either represents the flat band potential of n-GaAs, or is the effective potential of a surface level which, when reduced at more negative potentials, is totally effective in quenching the photocurrent. Further work must be carried out to resolve this issue.

D. Factors Influencing Photocurrents and Fill Factors

The other important features of Figure 3 are related to the photocurrents. For light intensities of up to 2.5 mW/cm^2, the photocurrents are limited by the number of photons absorbed by the n-GaAs, and thus by the number of holes produced. At the higher intensities, the photocurrents become limited by the supply of ferrocene to the electrode surface. An approximation of the steady state diffusional current is given by the Sand equation (9):

$$i(mA/cm^2) = \frac{nFCD}{1000\ \delta} \qquad (4)$$

where δ is the electrode separation ($\sim$0.04 cm), C is the concentration (in moles/cm^3) and D the diffusion coefficient. In the present case, $C = 6.3 \times 10^{-5}$ moles cm^{-3} and 10^{-5} is a reasonable value for D (11). The resulting limiting current is $\sim$1.5 mA/cm^2, which is close to our experimental observation. In a practical cell, a nearly tenfold increase in concentration would be necessary to support typical "solar cell" currents of 10-20 mA/cm^2. Similar results are obtained for the other redox couples.

---

*This is not surprising, since $MeOH/Br_2$ is a well-known etchant for GaAs.

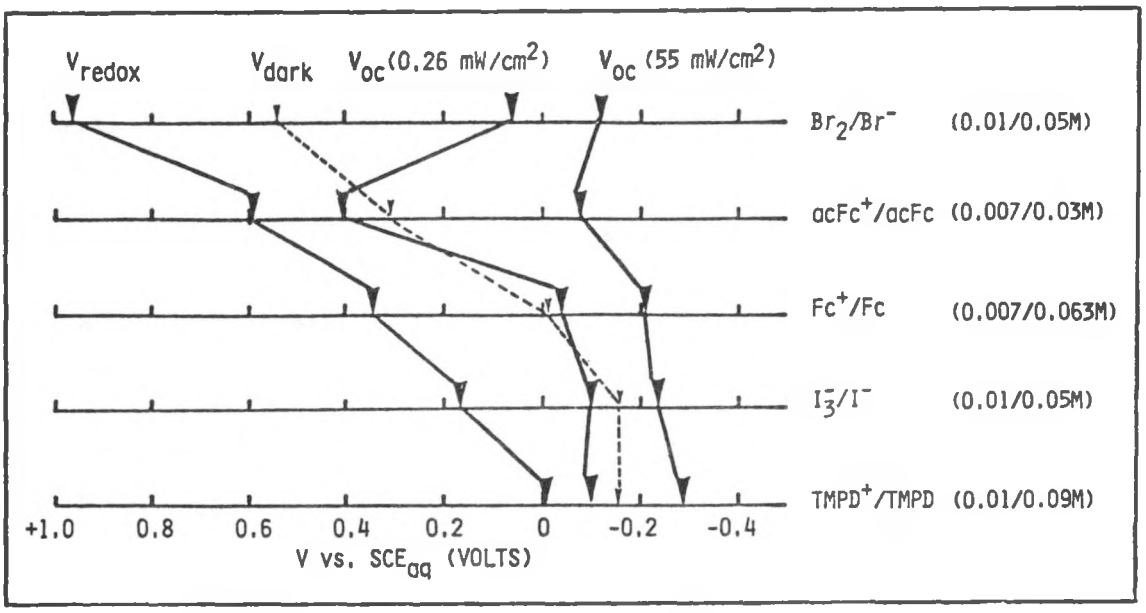

Fig. 6. Variations of V_{oc} and V_{dark} on a standard reference electrode scale, with a variety of redox couples in the cell n-GaAs/PC, 0.1M $LiAsF_6$, redox/NESA.

The fill factor or "squareness" of the current-voltage curves in the region between 0 volts and V_{oc} is an important variable in determining cell efficiencies. As shown previously in Figure 1, contributions to the final curve arise from polarizations at the photoelectrode and counter electrode, as well as from solution resistance. The production of photocurrent is also sensitive to the efficiency of light absorption, and to the lifetime of minority carriers. Cells based on n-GaAs/propylene carbonate, Fc^+/Fc (0.007/0.063M) have been tested in which we have varied the counter electrode, the concentration of supporting electrolyte, and the surface treatment of the n-GaAs. Some of the results are summarized in Table 4.

All cells listed in Table 4 exhibited diffusionally limited currents at high light intensities. Efficiencies in the range where currents were limited only by the hole flux, i.e., 0-2 mW/cm^2 white light, were 6-16% while efficiencies at solar intensities were <1.5%. The latter should be improved in more concentrated electrolytes. Short circuit photocurrents were enhanced by 25-30% by employing a black matte etched GaAs surface rather than a reflective shiny surface. Another increase in photocurrents was observed by decreasing the sheet resistance of the optically transparent counter electrode. NESA glass (SnO_x, 150 Ω-cm) gave short circuit currents which were about 50% less than the more conductive, though ∿20% less transmissive, NESATRON ($SnO_x \cdot In_2O_{3-x}$, 5 Ω-cm) gave short factors and efficiencies were also enhanced in the NESATRON cells, despite a reduction in voltage which may relate to NESATRON's higher optical absorption. An attempt to decrease the surface recombination velocity by adsorbing Ru^{+3} on the n-GaAs surface proved unsuccessful

TABLE 4

EFFECTS OF n-GaAs SURFACE TREATMENTS ON PERFORMANCE OF THE EPC n-GaAs|Fc^+(0.007M), Fc(0.063M), $LiAsF_6$(0.1M), PC|NESA OTE
FIGURES IN PARENTHESES ARE FOR NESATRON OTE

	Source Intensity (mW/cm^2) (150W Xe Arc, 300-1200 nm)		
Etch A	**0.9**	**6.7**	**53**
V_{oc} (V)	0.53	0.5	0.69
i_{sc} (mA/cm^2)	0.34	1.7	1.7
P_{max} (mW/cm^2)	0.08	0.23	0.28
η(%)	8.8	3.4	0.5
Etch B			
V_{oc} (V)	0.55 (0.46)	0.58	0.69 (0.59)
i_{sc} (mA/cm^2)	0.46 (0.69)	1.7	2.1 (2.91)
P_{max} (mW/cm^2)	0.12 (0.14)	0.26	0.44 (0.7)
η(%)	13.8 (15.6)	3.9	0.8 (1.32)
Etch C			
V_{oc} (V)	0.52	-	0.64
i_{sc} (mA/cm^2)	0.29	-	1.65
P_{max} (mW/cm^2)	0.08	-	0.24
η(%)	8.8	-	0.45

(surface treatment C, in the table). In the original work by Heller and co-workers, a Se^{-2}/Se_n^{-2} aqueous electrolyte was employed (3,4), and appears to be necessary for observation of the Ru^{+3} effect on photocurrent yields.

One major issue to be resolved in these and other n-GaAs cells is the true position of the flat band potential. Capacitance-voltage analysis indicate a flat band potential of -1.1 ± 0.2V vs. SCE, in agreement with Kohl and Bard in acetonitrile (14), although considerable frequency dependence characterizes the slope of the Mott-Schottky plots. Other estimates of V_{fb} can be made by observing the intersection of dark and light i-V curves (cf. Fig. 3) or by measuring the bias voltage at which the instantaneous photovoltage, obtained using a pulsed dye laser, is zero (Fig. 7). Both methods give a V_{fb} of only -0.2 to -0.3V. In addition, the plot of V_{oc} vs. V_{redox} shown in Figure 5 extrapolates to the same value of V_{fb}. Comparison with Table 2 indicates that, if the more positive values of V_{fb} are accepted, then the redox couples employed all have potentials lying within the n-GaAs gap. If the value of -1V is accepted, then several of the couples lie beneath the valence band edge, and it would be surprising if they could react with photogenerated holes. We have tested the stability of the n-GaAs cell with all the couples, and found over several hours operation that only the Br_2/Br^- cell shows significant degradation.

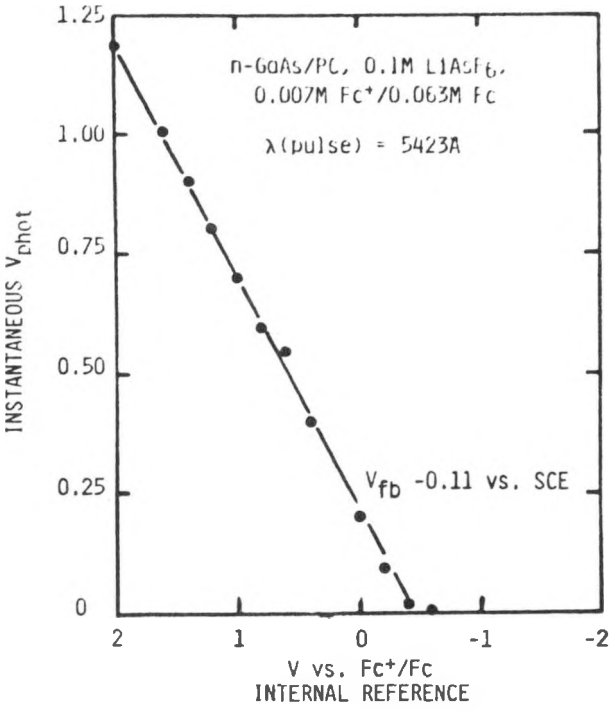

Fig. 7. Instantaneous photovoltage as a function of electrode bias.

E. Conclusions

We feel that some of the conclusions made possible by our work so far will be extremely valuable in cell design, particularly for the more economical thin film GaAs system. We have been able to make stable cells with V_{redox} up to +0.6V vs. SCE in propylene carbonate (e.g., acetyl ferrocene). Such cells have V_{oc} values of ∿0.7V. The limits of stability are exceeded with Br^-/Br_2 (+0.96V vs. SCE), so we estimate that the maximum V_{oc}'s attainable with stable cells in this solvent will be 0.7-1.0V. For such n-GaAs cells, relatively colorless, soluble redox couples must be developed with V_{redox} = 0.6-0.8V vs. SCE.

We have specified several ways to improve the photocurrent yields and fill factors in these cells. A polarizable counter electrode is essential, and NESATRON seems to be the best candidate so far for cells of the OTE geometry. The conductivity of propylene carbonate 1M $LiAsF_6$ or $LiClO_4$ is 7×10^{-3} Ω^{-1}-cm^{-1} (10). At current densities of 10 mA/cm^2, thicknesses of <0.1 mm must be employed to keep resistive voltage losses below 100 mV. Electrolytes more conductive than those based on propylene carbonate will probably be required, although some sacrifice in stability and hence maximum attainable V_{oc} may result.

Fill factors in these cells are limited by opposing dark currents. This situation is likely to be improved by decreasing the doping density and hence increasing the width of the space charge layer. In addition, fill factors are decreased by surface recombination, and chemical modification of surface defects by oxidation, hydrogenation or adsorption of metal ions is a possible solution.

III. n-GaAs ELECTROCHEMICAL PHOTOVOLTAIC CELLS EMPLOYING NONAQUEOUS IODIDE ELECTROLYTES

A. General Background

The results reported in Section I indicated that the iodine redox couple is worthy of further investigation for use in EPCs. The couple is economical and exhibits high solubility in both oxidized and reduced forms in a number of nonaqueous solvents, particularly as tetraalkylammonium iodide-iodine mixtures. The couple may be regeneratively oxidized and reduced.

The redox behavior of the iodine system shows very large solvent effects resulting from equilibria involving I_3^-. The dissociation constants of I_3^- are listed in Table 5 for several solvents. Protic solvents destabilize I_3^- while I_3^- remains largely associated in most aprotic media. The electrooxidation of I^- occurs in two separate steps in many aprotic solvents, corresponding to reactions (5) and (6):

$$3I^- \rightarrow I_3^- + 2e \qquad (5)$$

$$2I_3^- \rightarrow 3I_2 + 2e \qquad (6)$$

In protic solvents, the oxidation occurs in one step, due to the reduced stability of I_3^-. The potentials corresponding to reactions (5) and (6) also vary with solvent as indicated in Table 6. These data suggest that both the choice of solvent and the ratio of I^- to I_2 might have a profound effect on photoelectrochemical cell parameters.

TABLE 5

VALUES OF $pK_{diss} = -\log([I_2][I^-]/[I_3^-])$ IN SEVERAL NONAQUEOUS SOLVENTS. (Data compiled from R. Alexander, E.C. Ko, Y.C. Mae and A.J. Parker, J. Am. Chem. Soc., 89, 3703 (1967).)

Solvent	pK_{diss}
H_2O	2.85
$HCONH_2$	3.7
CH_3OH	4.30
CH_3CN	6.6
DMSO	6.9
DMF	7.0
DMAC	7.4

TABLE 6

VALUES OF $E_{\frac{1}{4}}$ vs. SCE FOR OXIDATION OF I^- IN NONAQUEOUS SOLVENTS.
(Data compiled from R. Iwamoto, Anal. Chem., 31, 955 (1959)(15).)

Solvent (0.1M $NaClO_4$)	$E_{\frac{1}{4}}$ (Rxn.[5])	$E_{\frac{1}{4}}$ (Rxn.[6])
Water	0.51	-
Methanol	0.40	-
1-Butanol	0.42	-
2-Propanol	0.42	-
Acetic Acid	0.44	-
Ethylene Glycol	0.42	0.52
Pyridine	0.37	-
Acetonitrile	0.25	0.55
Acetone	0.22	0.62
Acetic Anhydride	0.20	0.60
1,2-Dimethoxyethane	0.39	0.65
Dimethyl Sulfoxide	0.48	0.70
1:1 Acetone/Water	0.42	0.54
1:1 Ethylene Glycol/1,2-Dimethoxyethane	0.37	0.56

B. Experimental Methods

1. Electrode Materials. The n-GaAs single crystal electrodes prepared for use in the experiments are listed in Table 7. Electrodes of 100, 110, and 111 orientation were provided with ohmic contacts by rubbing GaIn eutectic #60 (Indium Corp. of America) on the back surface and attaching a Ni disc and wire with Ag epoxy. The wire was threaded through a glass capillary and all but the front face of the crystal insulated with G.C. epoxy.

TABLE 7

n-GaAs ELECTRODES EMPLOYED IN THIS WORK

Orientation	Area (cm^2)	Dopant	Resistivity (Ω-cm)	Source
100	0.07,0.113	Si-Zn Compensated	0.11	W. W. Harvey
110	0.111	Si-Zn Compensated	0.11	W. W. Harvey
111	0.139	Si	$\sim$0.1	Atomergic, XL #5-80

Etch methods reported in the literature for GaAs have been shown to leave varying thicknesses of native oxide on the crystal surface (16). Surface preparation also has a large effect on short circuit photocurrent and fill factor in EPCs. Most of the literature information deals with <100> face orientation of single crystal GaAs although there is occasional mention of <111> orientation. All possible orientations will be present in polycrystalline GaAs. Therefore, it is necessary to determine the best overall etch method to enhance fill factors on each face and to minimize any deleterious effects which may occur on any specific face.

Initial experiments were performed on crystals which were polished with Buehler alumina of increasingly fine mesh, the last of which was 0.03μ particle size. Such polishing was expected to produce a high density of surface states and therefore the baseline from which all other surface treatments will be judged. The "fast" etch method, using 1:1 H_2O_2:H_2SO_4 (17) to produce a matte black surface on all three crystals, was also used. Other methods which result in surface oxides of lesser thickness will be investigated subsequently.

2. Electrolyte Solutions. Initial experiments in PC (Section D below) were carried out using Li^+-containing electrolytes discussed in Section II. Further experiments on iodide-based EPCs were performed using the nonaqueous I_3^-/I^- solutions shown in Table 8. These were prepared from deaerated anhydrous solvents and anhydrous tetrabutylammonium tetrafluoroborate ($TBABF_4$) in which was also dissolved 0.1M I_2 and 0.1M tetrabutylammonium iodide (TBAI). The preparation and handling of solutions

was carried out in an Ar atmosphere glove box containing <5 ppm H_2O. Solution resistances were measured in a conductivity cell using a General Radio 1650-B impedance bridge, operated at 1 kHz. The solutions are listed in Table 8 in order of increasing conductivity. In general, the specific conductance of the solutions does not increase with the addition of the iodide redox couple to the supporting electrolyte at these high concentrations. The only exception is propylene carbonate, the solvent with the highest dielectric constant, indicating that ion pair formation may be an important factor in some of these solvents. The methanolic solution concentrations are not comparable to the other solutions because I_2 is not as soluble in MeOH. Estimated concentration of this solution is 0.1M TBAI and 0.04M I_2. The absorbance of the resulting solutions at 360 nm indicates that the dissociation constant for I_3^- must be of the same order of magnitude as that reported for acetonitrile ($K_d = 1 \times 10^{-7}$)(18) in all solvents except anhydrous methanol.

3. Photoelectrochemical Evaluation. Initial experiments in PC were conducted as described in Section II. In the remaining experiments, which involved the surveying of many electrode/electrolyte combinations, the simple cell design shown in Figure 8 was employed. Unless noted otherwise, half cell measurements were employed to isolate the polarization behavior of the photoelectrode. An internal Pt indicator electrode was used as a reference electrode. In each solution, the Pt/redox reference potential was measured vs. a Li^+(1M)/Li electrode in PC with a microporous liquid junction. These potentials as well as their potentials vs. SCE_{aq} are listed in Table 9.

Photoelectrochemical measurements were performed in the glove box by irradiating through a window. Illumination was carried out as previously described or with a He-Ne laser diffused so the beam covered the electrode surface. Light intensity impinging on the cell was measured radiometrically within the glove box. Electrodes were placed 0.5 cm from the cell window. Measurements of the optical density of the solutions at 623.8 nm indicated a solution transmittance of about 16% for the 0.5 cm path length. An intensity of about 0.8 mW/cm^2 was calculated at the semiconductor surface. Current-voltage curves were measured using standard electrochemical equipment.

C. n-GaAs EPCs in Propylene Carbonate/Iodide Electrolytes

Initial experiments were carried out to determine the photoelectrochemical behavior of n-GaAs in contact with solutions of PC, $LiClO_4$ containing various concentrations and ratios of I^- and I_2. The purpose of the investigation was to determine the compositional effects on photovoltage and photocurrent in this system. The specific solutions employed are listed in Table 10. Reversible potentials of each solution were measured vs. a Li^+/Li reference electrode and are also included in Table 10. It is evident that equimolar solutions of I^- and I_2 are dominated by the more positive I_2/I_3^- redox potential (reaction 6), while an excess

TABLE 8

SPECIFIC CONDUCTANCE OF 1M SOLUTIONS OF $TBABF_4$ IN SOME ORGANIC SOLVENTS

Solvent	Dielectric Constant	Viscosity at 25°C (cp)	Specific Conductance, $\Omega^{-1}cm^{-1}$			Conc. I_3^- from Absorbance at 360 nm $\varepsilon_{360} = 2.9 \times 10^4$
			T,°C	1M $TBABF_4$	0.1M I_2, 0.1M I^- Added	
Propylene Carbonate	64.4	2.53	22.2	0.0064	0.0066	0.098M
Methyl Formate	8.5	0.33	23.3	0.0099	0.0099	0.087M
Dimethyl formamide	36.7	0.802	22.2	0.0139	0.0135	0.082
Anhydrous* Methanol	37.5	0.59	23.3	0.0152	0.0148*	0.037*
Acetonitrile	38.0	0.345	22.2	0.0317	0.0298	0.093

*I_2 was not soluble to 0.1M in MeOH.

TABLE 9

EPC CELL PARAMETERS FOR n-GaAs HALF CELLS IN SEVERAL NONAQUEOUS SOLVENTS WITH 1M $TBABF_4$, 0.1M TBAI/0.1M I_2. He-Ne INTENSITY ~0.8 mW/cm^2

Solvent	Specific Conductance ($\Omega^{-1}cm^{-1}$)	Actual Conc.* $[I_3^-]$ (moles/ℓ)	$[I^-]$ (moles/ℓ)	Potential Pt/redox vs. Li+/Li (volts)	Potential Pt/redox vs. SCE (volts)	Electrode Orientation					
						n-GaAs <100>		n-GaAs <110>		n-GaAs <111>	
						V_{oc}	I_{sc}/cm^2	V_{oc}	I_{sc}/cm^2	V_{oc}	I_{sc}/cm^2
Propylene Carbonate	0.006	0.098	0.002	+3.121	+0.178	-0.365	0.39	-0.33	0.11	-0.495	0.11
Methyl Formate	0.0099	0.087	0.013	+3.064	+0.121	-0.27	0.28	-0.23	0.1	-0.46	0.05
Dimethyl-formamide	0.0135	0.082	0.018	+2.985	+0.042	-0.44	2.74	-0.42	1.23	-0.46	0.9
Acetonitrile	0.0298	0.093	0.007	+3.307	+0.364	-0.37	1.28	-0.29	0.14	-0.39	0.107

*Determined spectrophotometrically, $\varepsilon_{360} = 2.9 \times 10^{-4}$ for I_3^-.

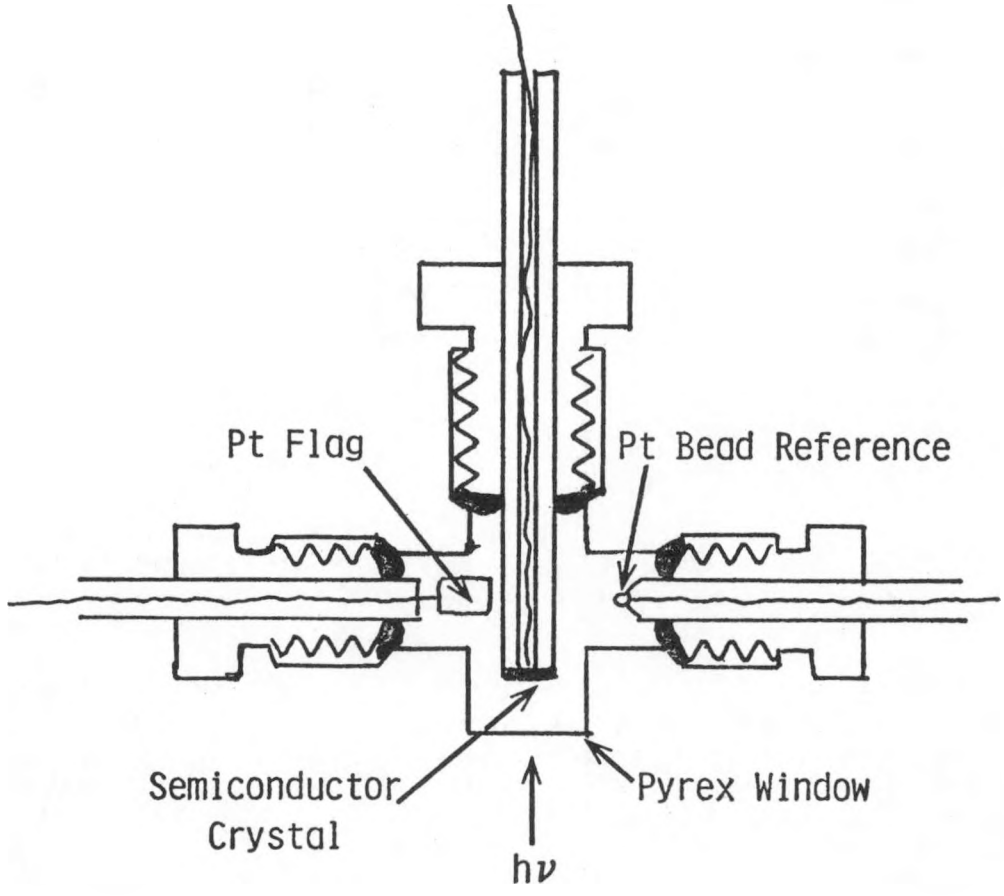

Fig. 8: Top view of electrolyte evaluation cell.

of I^- results in a considerably more negative rest potential characterized by reaction 5.

TABLE 10

COMPOSITIONS OF IODIDE ELECTROLYTES IN PROPYLENE CARBONATE, AND THEIR MEASURED REVERSIBLE POTENTIALS ON Pt

	$[I^-]^*$	$[I_2]^*$	$[Li^+]$	E(vs. Li^+/Li)	E(vs. SCE)
1:1A	0.05	0.05	0.15	3.58	+0.66
1:1B	0.025	0.025	0.125	3.59	+0.65
1:1C	0.0125	0.0125	0.112	3.59	+0.65
1:5A	0.05	0.01	0.15	3.11	+0.167
1:5B	0.025	0.005	0.125	3.13	+0.187
1:5C	0.0125	0.0025	0.112	3.15	+0.207
1:10A	0.05	0.005	0.15	3.10	+0.157
1:10B	0.025	0.0025	0.125	3.12	+0.187
1:10C	0.0125	0.00125	0.112	3.14	+0.197

*Formal concentration as prepared. The real concentrations in the solutions depend on the dissociation constant of the I_3^- which we estimate to be $<10^{-5}$ in PC.

Open circuit photovoltages of cells based on the solutions in Table 10 are recorded in Figures 9 and 10 as a function of light intensity. We find that the photovoltages of these cells are highly anomalous and irreproducible compared to the cells based on the ferrocene derivatives reported on earlier. For example, we might expect the value of V_{oc} to be larger for the 1:1 I_2/I^- solutions compared to the 1:5 and 1:10 solutions, based on their observed redox potentials. However, the results in Figures 9 and 10 indicate no large effects of composition on photovoltage. Another anomaly is the maximum obtained in the photovoltage-intensity curves at intermediate light intensities. This maximum was observed for nearly all cells in the series, and is as yet unexplained. It may involve a photoinduced adsorption between an electrolyte species and the electrode surface or may in some way be influenced by I_3^- oxidation which occurs at intermediate and high light intensities (vide infra).

In many of the iodine cells, the photovoltage showed much less variation with light intensity than with the ferrocene or acetylferrocene couples. The current-voltage behavior of such cells, typified by the data in Figure 11, show clearly such an invariant voltage of photocurrent onset. Although for simplicity we did not

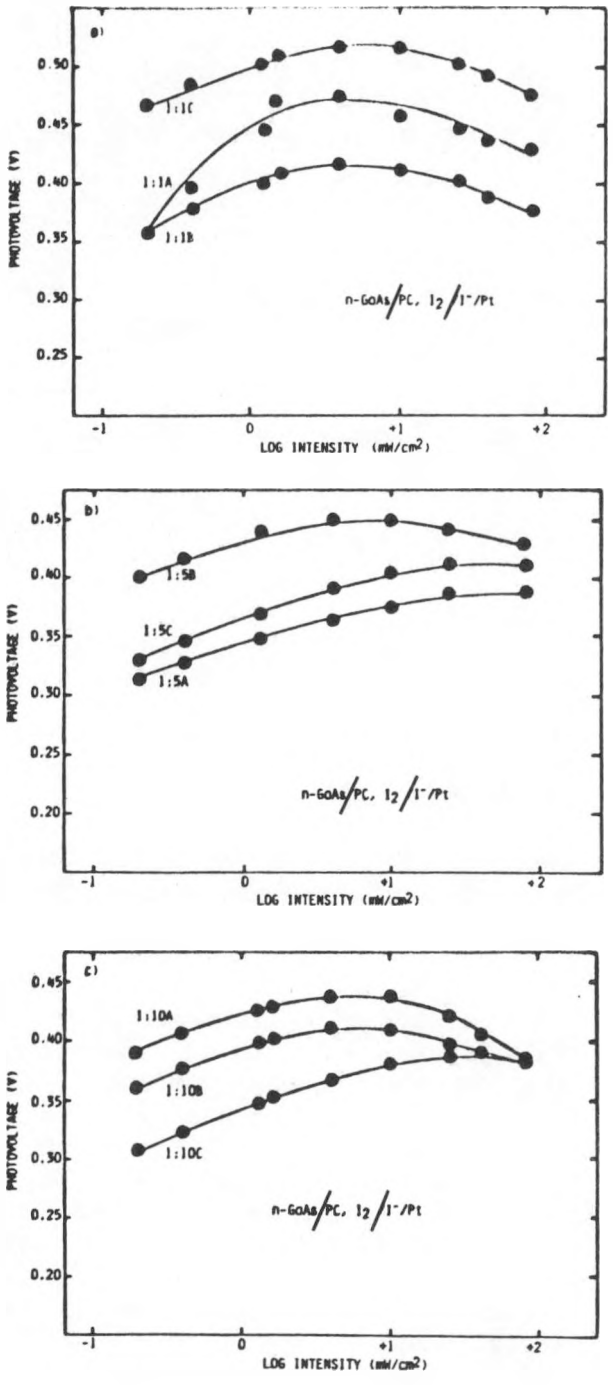

Fig. 9: Intensity dependence of open circuit photovoltages of n-GaAs EPCs utilizing various ratios of I_2 and I^- in propylene carbonate.

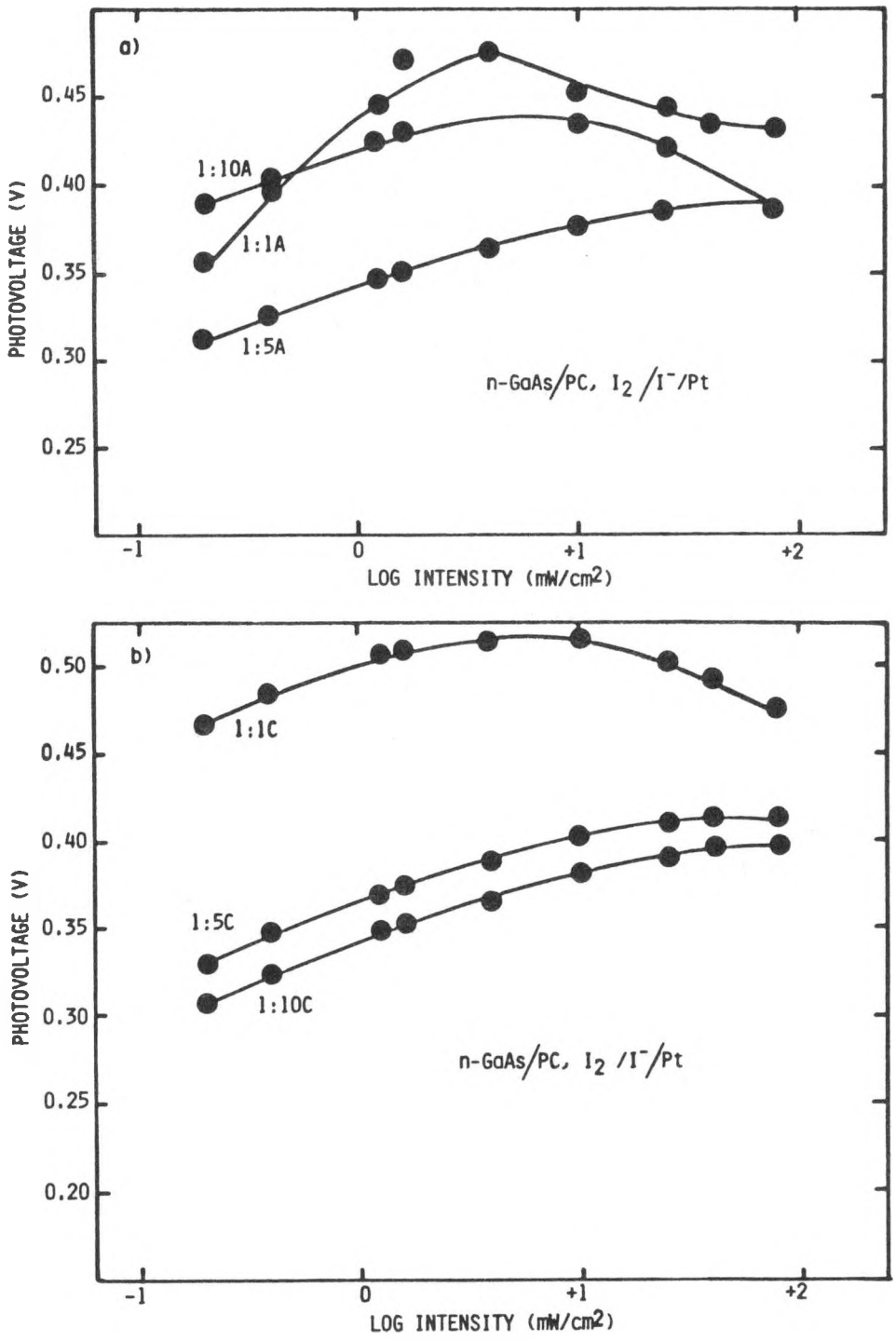

Fig. 10: Effects of I_2/I^- ratios on photovoltages in n-GaAs EPCs at constant $[I^-]$. a) $[I^-] = 0.05F$; b) $[I^-] = 0.012F$.

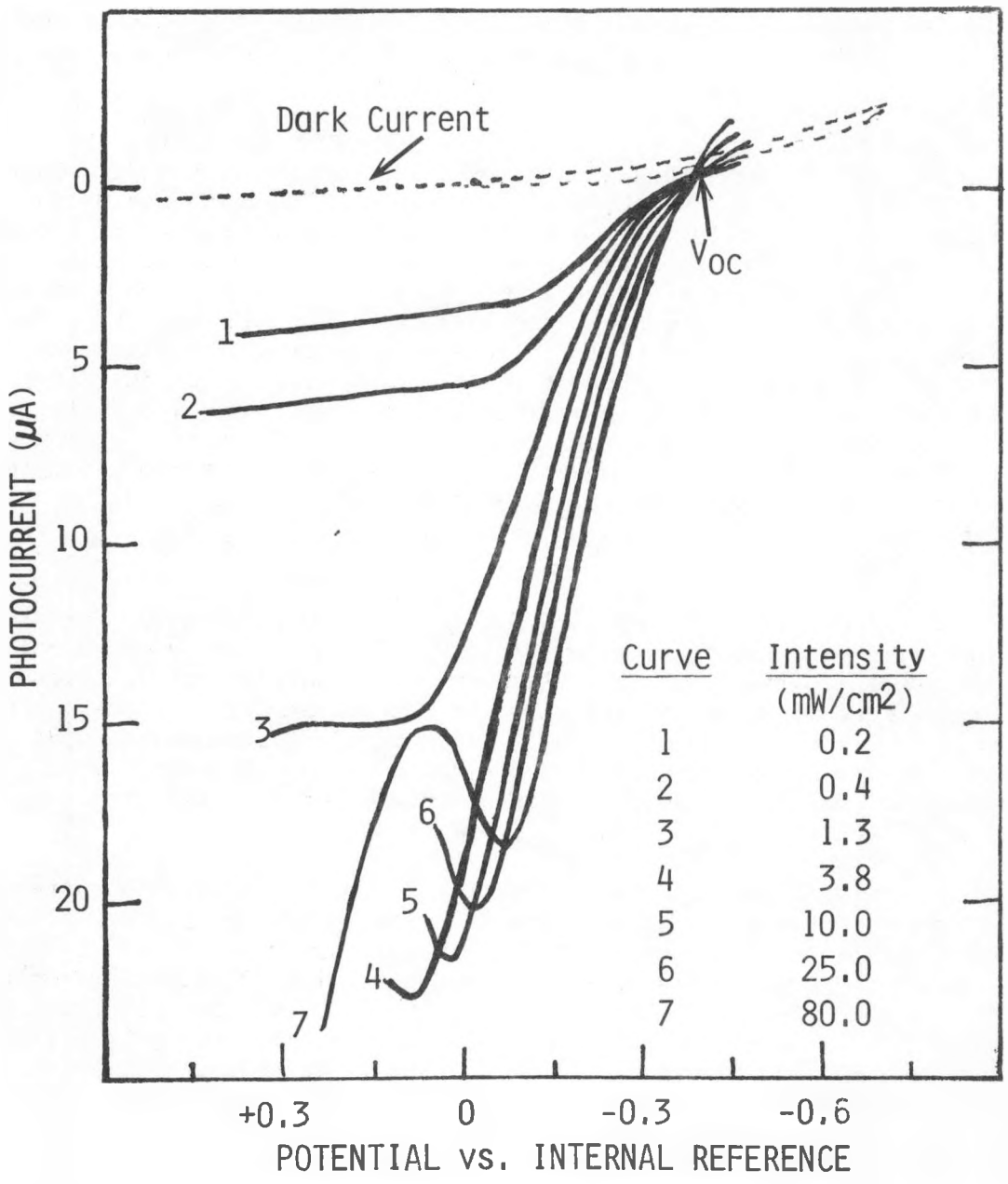

Fig. 11: Photocurrent as a function of light intensity for the half cell: n-GaAs/solution 1:10C/Pt. Internal reference is +0.197 vs. SCE_{aq}. Exposed area of the n-GaAs crystal is 0.07 cm^2.

show it on Figure 11, a second anodic peak was found in all solutions at more positive bias and at light intensities greater than 3.8 mW/cm^2.

The short circuit photocurrents for the n-GaAs half cells are plotted in Figures 12 and 13 as a function of light intensity. At low intensities, photocurrents are hole limited and relatively independent of redox concentration. At high intensities, the currents are diffusionally limited, the relative currents being more or less proportional to I^- concentration. According to Figure 13, the currents are not affected by the I_2/I^- ratio. At intensities above 3.8 mA/cm^2, a second anodic oxidation is observed at more positive potential than the first. This may be due to oxidation of I_3^- (reaction 6) present in the bulk solution as well as that formed at the electrode surface in the first wave (reaction 5). At high intensities, I^- will be quickly depleted at the SC surface and holes may then react with I_3^-. Since photocurrents for both oxidations are dependent on concentration of the redox couple at any given redox ratio, both I_3^- and I^- oxidation must favorably compete with photoanodic dissolution.

In general, currents obtained for these cells are lower than those obtained for ferrocene or for TMPD cells in the same solvent. This is possibly caused by sluggish redox kinetics of the iodide redox reactions in propylene carbonate, or to a high surface recombination rate caused by a high density of interface states. The latter would also explain the relatively invariant photovoltages. Exchange of electrons can occur between surface states and the redox species, being manifested as a "pinning" of the Fermi level, commonly experienced in solid state Schottky barrier devices.

A series of 3-4 hour runs were made on the cells with the more concentrated redox electrolytes (the A series in Table 10). To obtain maximum currents and to accelerate the test, cells were biased at +0.3V vs. the internal reference scale, and were illuminated with 80 mW/cm^2 white light. Under these conditions, reaction (6) is most likely. After an initial decrease in photocurrent due to electrode polarization, currents were unchanging over the test period. We note that n-GaAs rapidly passivates in PC electrolyte without the I^- or I_3^-, indicating the stabilizing nature of the redox couple.

D. Solvent and Orientation Effects on n-GaAs EPC Operation

Figure 14 shows comparative photocurrent voltage curves for EPCs of the general configuration

n-GaAs/solvent, 0.1F TBAI, 0.1F I_2

Results are given for <100>, <110>, and <111> crystalline faces.

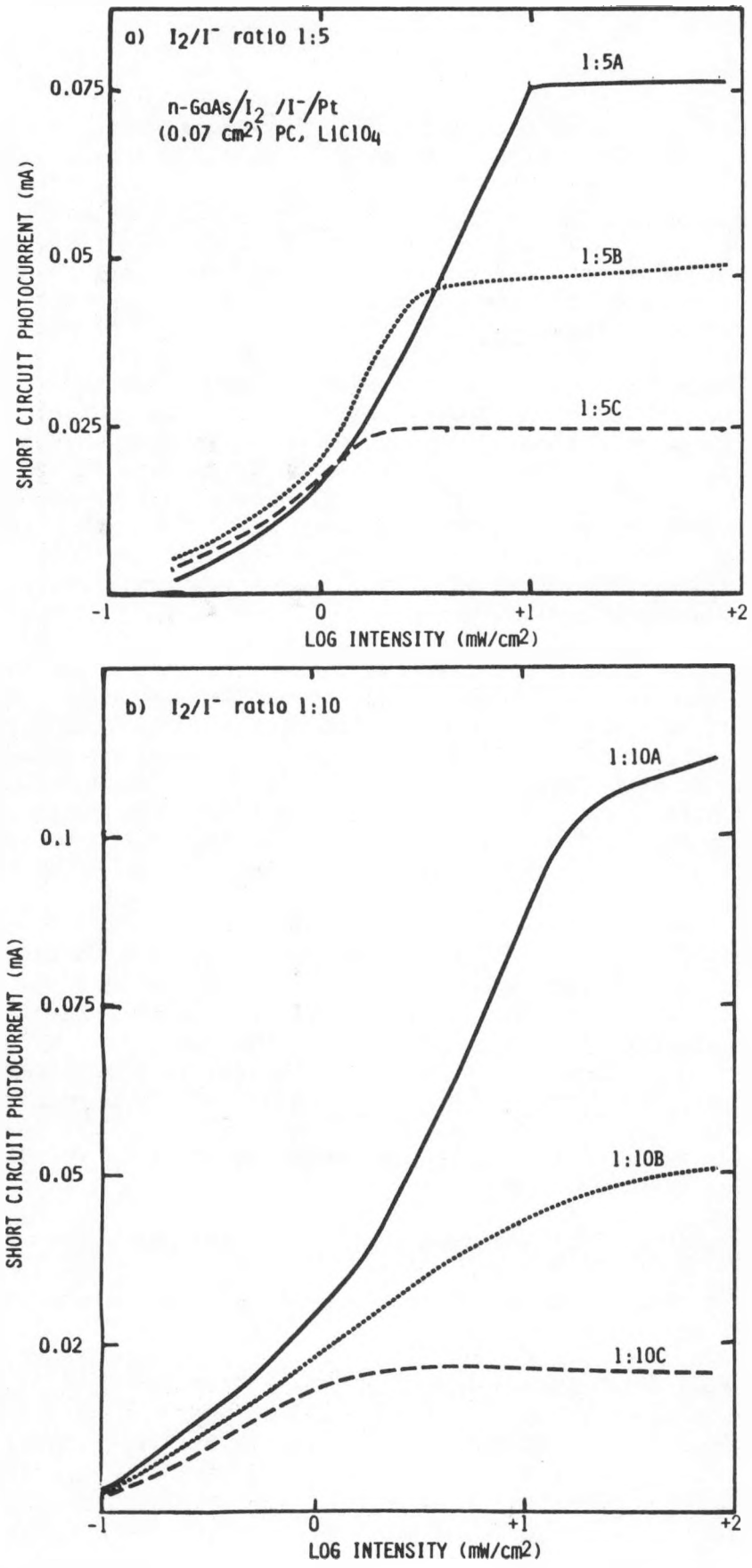

Fig. 12: Photocurrents as a function of redox couple concentration at constant I_2/I^- ratio. See Table 1 for solution compositions.

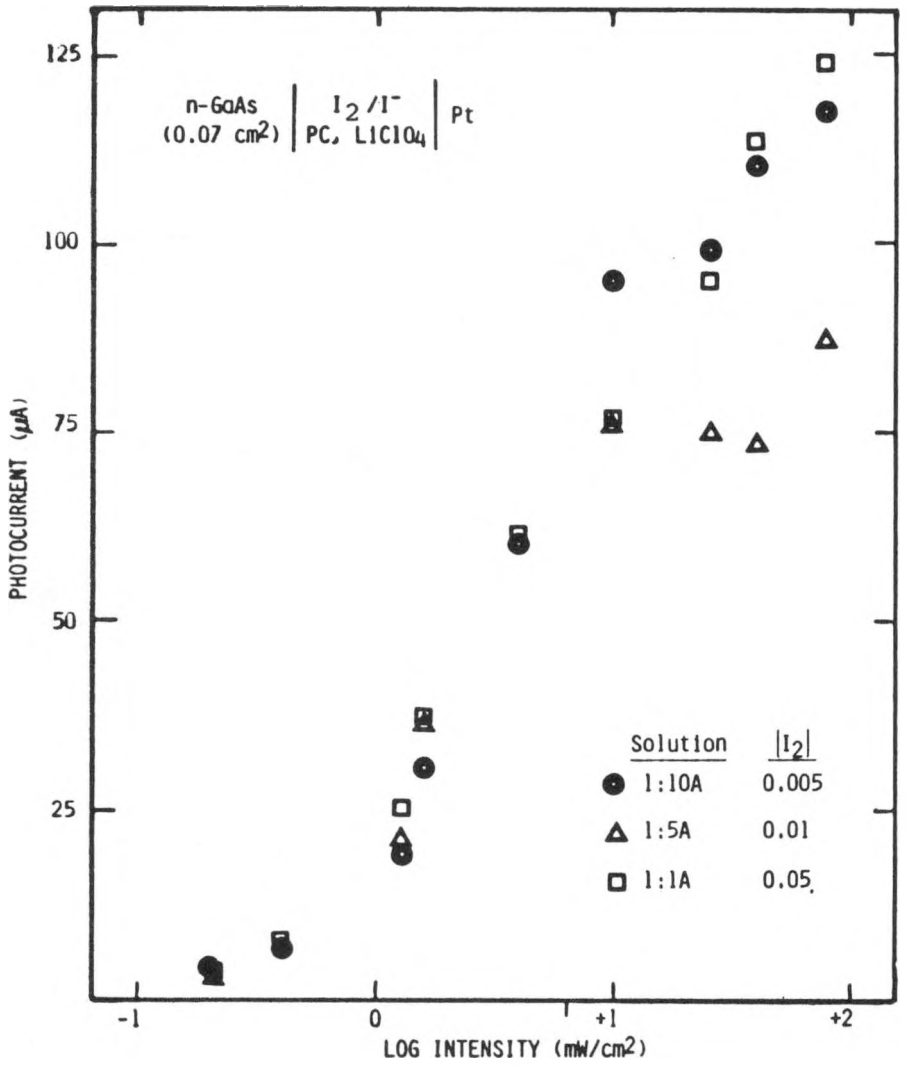

Fig. 13: Effect of iodine concentration on photocurrent, at constant $[I^-] = 0.05F$.

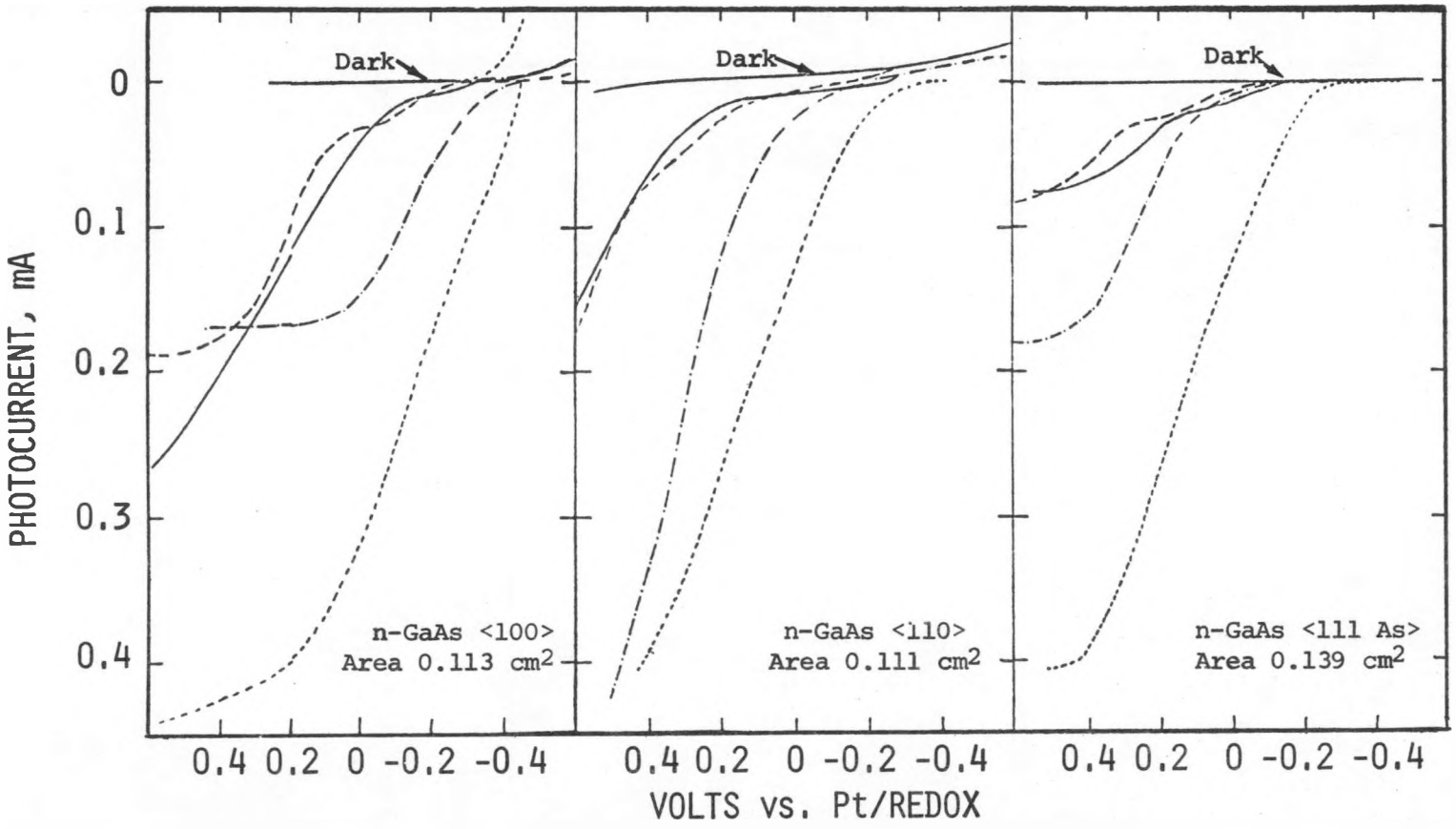

Fig. 14: Photocurrent vs. voltage-curves for polished n-GaAs single crystal electrodes of different orientations in several nonaqueous solvents. Half cell measurements of the cell: n-GaAs|nonaqueous solvent, 1M $TBABF_4$, 0.1M TBAI/0.1M I_2|Pt. (Values of Pt/redox in each solvent are given in Table 1.) Illumination by He-Ne laser at ∿0.8 mW/cm^2. Solvents: —— Propylene carbonate, --- Methyl formate, -.-.- Acetonitrile, ... Dimethylformamide.

Inspection of the curves in Figure 14 shows that photocurrents for DMF are much larger than in the other three solvents at the particular concentrations of I^- and I_2 used to make up the solutions. The low specific conductance in PC and slow electron transfer rates (19) in PC and MF probably account for the small photocurrent densities exhibited relative to those in DMF and AN. On the other hand, the superiority of DMF over AN is not a matter of solution conductance but may be due to contributions from anodic dissolution in DMF (see below).

Some effects of electrode orientation are evident in Figure 14. The <100> face electrode has the largest dark currents in all four solvents. The <111> face electrode shows little or no dark current out to -0.6V vs. Pt/redox. The <110> face electrode shows intermediate behavior. In all solvents, the <111> electrode thus gives the largest V_{OC}, since the photoanodic current is not required to overcome a large cathodic back reaction as is the case on the <100> face.

Short circuit photocurrent densities listed in Table 9 show the definite superiority of the <100> face orientation over the other two in all solvents.

All three electrodes were matte etched in 1:1 H_2O_2:H_2SO_4, and the effect of the etch treatment evaluated in the DMF electrolyte. Figure 15 shows that the fill factor definitely improves for the <111> electrode. There is a small change in the <110> and on the <100> face, where we have previously seen improvement with this type of etch, in that we note a change in the shape of the curve and a decreased i_{sc}.

E. Effects of I^- on n-GaAs Photodecomposition in Nonaqueous Solvents

The photodecomposition of a matte etched n-GaAs electrode was studied in PC, AN, and DMF solutions containing 1M $TBABF_4$. A 5.3 mW/cm^2 He-Ne source was used to illuminate the semiconductor in a half cell with a Pt flag counter electrode and a Li^+(1M, PC)/Li in a Luggin capillary as the reference electrode (E° vs. SCE -2.943V). After recording the photooxidation curve, the electrode was removed and reetched, 1 ml of the solvent containing 0.1F I_2, 0.1F TBAI, and 1M $TBABF_4$ was added to the cell making the solution $\sim$0.02F in I_2 and TBAI. The current-voltage behavior was recorded again. Because of absorbance of I_3^- at 638.2 nm, the light intensity was somewhat attenuated. Figure 16 shows the photocurrents recorded before (A) and after (B), the addition of the redox couple.

Current vs. time curves were also recorded with and without redox couple at the same bias voltage.

1. PC and AN. Time vs. current curves without redox couple present show a rapid decay of photocurrent to very low values which may be ascribed to the buildup of a resistive layer on the semiconductor

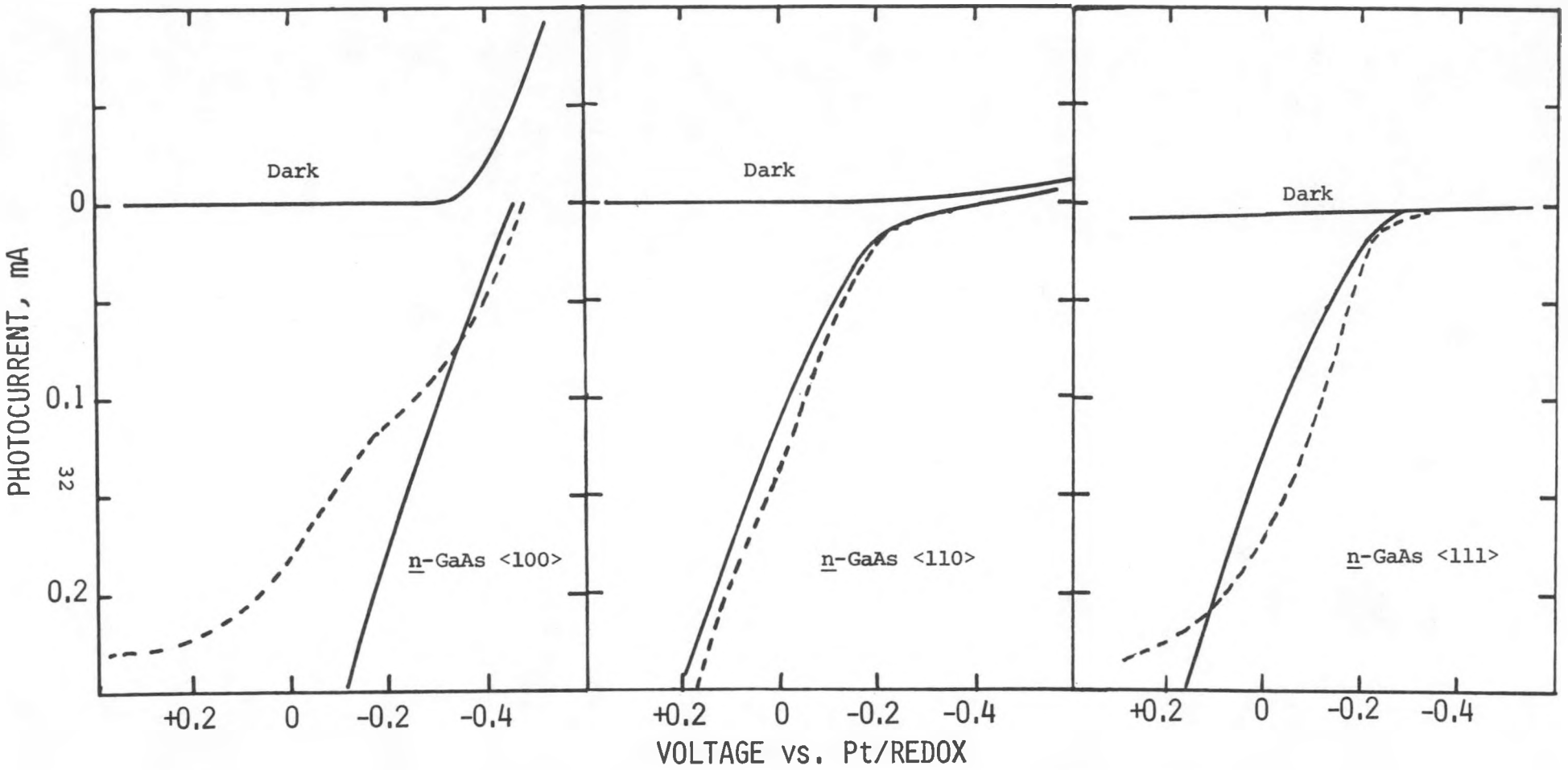

Fig. 15: Effect of matte etch treatment on n-GaAs electrodes of different surface orientation. Half cell: n-GaAs|DMF, 1M $TBABF_4$, 0.1M TBAI/0.1M I_2|Pt. ——— Polished surface, ----- matte etched in 1:1 H_2O_2:H_2SO_4. Illumination 0.85 mW/cm^2 He-Ne laser.

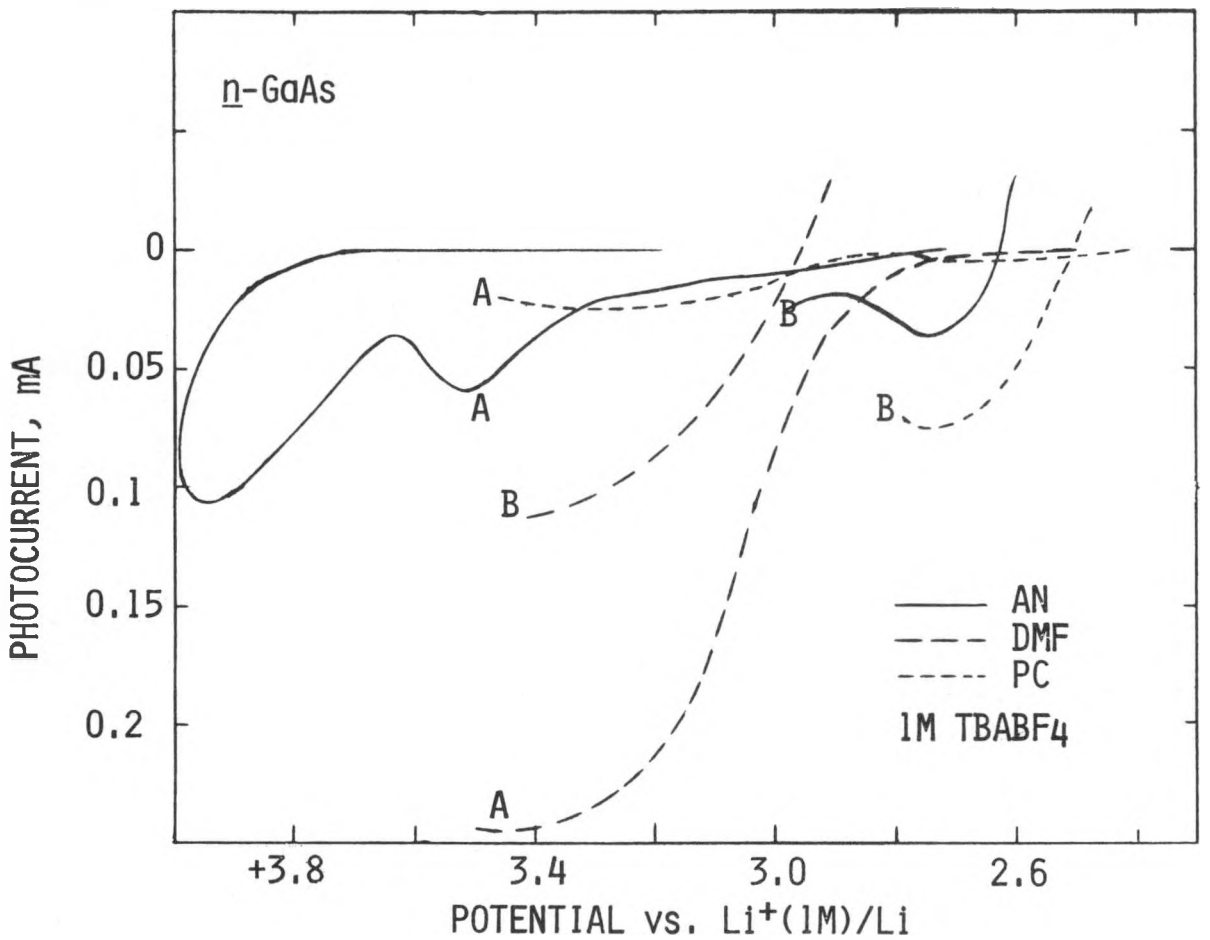

Fig. 16: Effect of addition of I_3^-/I^- redox couple on n-GaAs photodissolution. Curves A, without, Curves B, with added redox couple, approximately 20 mM in I_2 and I^-. Excitation: 5.3 mW/cm^2 He-Ne. Crystal etched between runs with 1:1 H_2O_2, H_2SO_4.

surface. In the presence of a small amount of redox couple, however, a steady-state photocurrent, i_{ss}, is maintained even in the unstirred cell (see Figure 17). When the solution is stirred, the peak current i_p is maintained. We interpret this to mean that the drop in current from i_p to i_{ss} is due to concentration polarization of the cell and that I^- oxidation competes effectively with photopassivation of the n-GaAs electrode. Figure 16 also shows that the photocurrent is higher at more positive potentials when the redox couple is added, for both PC and AN solvents.

2. DMF and MeOH. In contrast to PC and AN, the large photocurrent in DMF without redox couple shown in Figure 16 does not decay with time and therefore indicates a facile dissolution (oxidation/solvation) reaction. At the low concentration of I_2 and I^- added in this experiment, there is only a slight suppression of dissolution, possibly due only to reduced light intensity at the semiconductor surface caused by I_3^- absorbance. It appears, however, that at higher I^- concentration (see Figure 18) oxidation of I^- does occur at the illuminated GaAs surface. Similar indications of electrode instability were noted for MeOH/I^--based electrolytes.

F. Effect of I^- Concentration on Photocurrent

Experiments reported above with n-GaAs and the I_3^-/I^- redox couple suggested that decreasing the I_2 concentration relative to I^- would result in higher short circuit currents both by reducing the solution absorbance due to I_3^- and increasing the free I^- availability for reaction with photoproduced holes.

The solutions listed in Table 11 were prepared and the specific conductance, absorption spectra, and potentials determined, as previously described. Half cell measurements vs. Pt/redox were obtained using a low power (5.3 mW/cm^2) He-Ne laser for solutions in AN and DMF. Figure 18 shows the results of the photocurrent-voltage curves on the same matte etched, <100> face n-GaAs electrode for the AN and DMF electrolytes (B curves) compared to results reported previously for equimolar solutions of I_2 and I^- (A curves) where there is very little free I^- ion to be oxidized due to formation of I_3^-. The expected increase in i_{sc} with increase in I^- ion concentration and decrease in solution absorbance does occur. The effect is most pronounced in AN where an i_{sc} of 4.42 mA/cm^2 at an intensity 4.2 mW/cm^2 (632.8 nm, corrected for solution absorbance) is produced. For this cell, a power efficiency of 17.9% (ff = 0.34) is achieved at -0.2V vs. Pt/redox. It should be possible to improve this even more by increasing the TBAI concentration relative to the I_3^- concentration, subject to the considerations of the counter electrode reaction (see following sections).

G. n-GaAs/Acetonitrile, I_3^-/I^-/Pt Cells

Data for n-GaAs half cells in which the concentration of I^- was varied from 1 x 10^{-3} to 1.0 molar are listed in Table 12. The concentrations

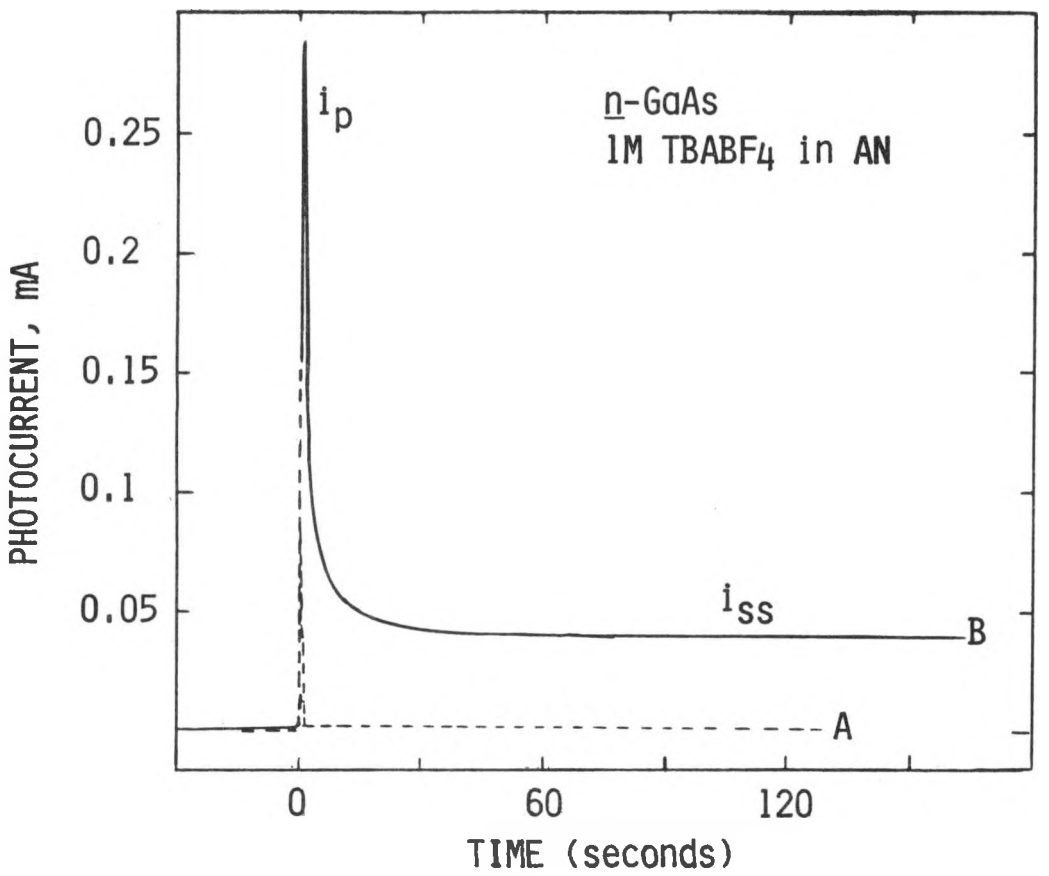

Fig. 17: Photocurrent vs. time curve for n-GaAs in AN, potentiostated at +2.84V vs. Li^+/Li. Curve A, no redox couple. Curve B, approximately 20 mM in I_2 and I^-. Excitation 5.3 mW/cm^2 He-Ne.

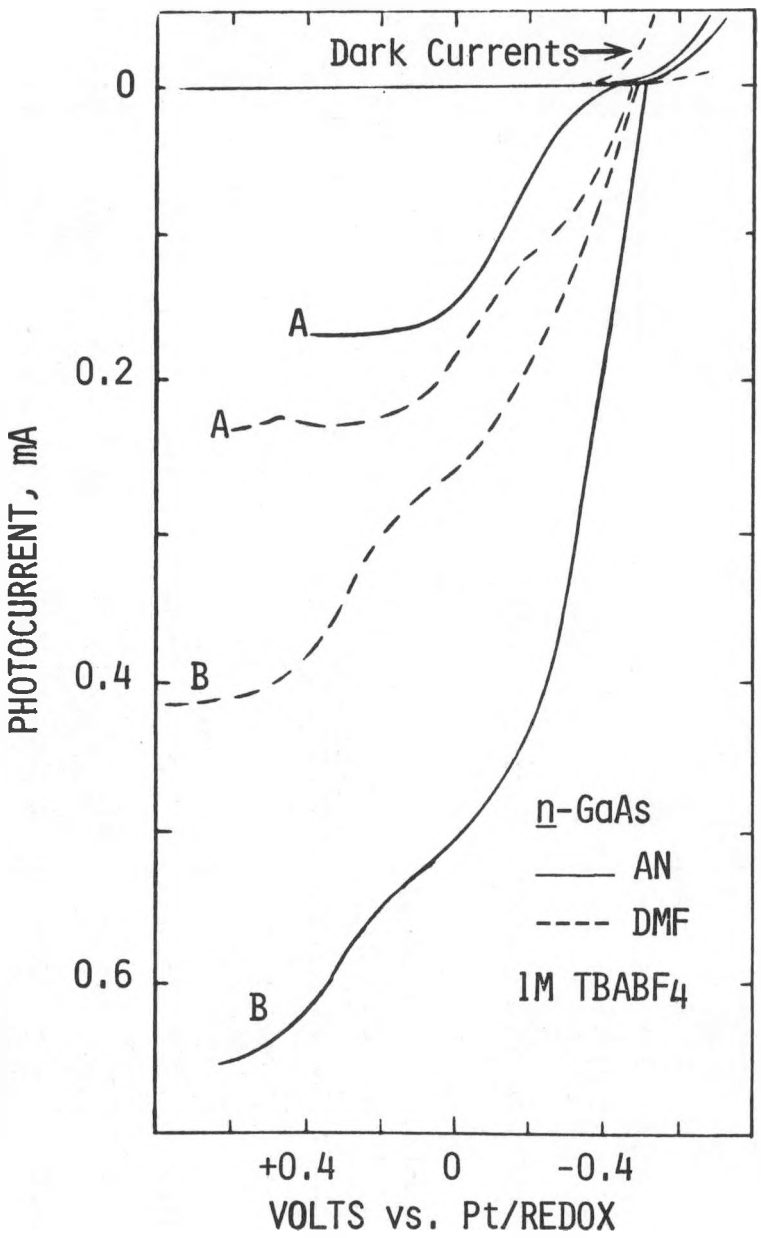

Fig. 18: Photocurrent vs. voltage curves for n-GaAs (area 0.113 cm^2). Excitation: 5.3 mW/cm^2 He-Ne. Curves A, 0.1F I_2, 0.1F TBAI. Curves B, 0.01F I_2, 0.11F TBAI. For actual concentrations of I_3^-/I^-, see Table 1. For AN-B, power efficiency is 17.9% corrected for solution absorbance at 632.8 nm.

TABLE 11. PROPERTIES OF I_3^-/I_3 SOLUTIONS EMPLOYED IN EPC INVESTIGATIONS.

Solvent	Supporting Electrolyte	Redox Couple Added		Specific Conductance ($\Omega^{-1}cm^{-1}$)	Actual Conc.* I_3^-	E_{redox} vs. SCE	% T for 5 mm Path Length at 632.8 nm
		I_2	I^-				
DMF	1M $TBABF_4$	0.01F	TBAI, 0.11F	0.0137	0.0134	-0.036	78.2
AN	"	0.01F	TBAI, 0.11F	0.0305	0.0125	-0.007	79.5
MeOH	"	0.01F	TBAI, 0.11F	0.0164	0.0092	+0.165	81.4
H_2O	1M $HClO_4$	0.01F	KI, 0.11F	0.3246	0.0077	-	83.1

*Determined spectrophotometrically.
$\varepsilon_{363} = 2.94 \times 10^4$ for I_3^-.
$\varepsilon_{363} = 2.64 \times 10^4$ in aqueous solution.

TABLE 12. n-GaAs HALF-CELL CHARACTERISTICS FOR ACETONITRILE SOLUTIONS OF TBAI, IODINE.

Cell No.	Actual Concentrations			Solution Resistivity	Light Source Intensity	Half-Cell Output					Current-Time Behavior†	
	I^-	I_3^-	$TBABF_4$	(Ω-cm)	(mW/cm^2)	V_{oc} vs. Pt/redox	i_{sc} (mA/cm^2)	Max. Power (mW/cm^2)	η (%)	f.f.	NR Stirred	NR Unstirred
1	0.001	0.02	1.0	31.5	HeNe(5.3) 632.8 nm	-	-	-	-	-	-	-
2	0.007	0.093	1.0	33.55	" (5.3)	-0.37	1.28	0.115	2.1	0.24	-	-
3	0.10	0.012	1.0	32.78	" (5.3)	-0.48	4.42	0.77	14.6	0.36	0.47	0.30
4	1.0	0.01	0	32.8	" (5.3)	-0.485	5.11	0.94	17.7	0.42	0.05	0.05
					Xe, 765 nm (0.5)	-0.409	0.292	0.035	7	0.29	-	-
					Xe, pyrex, H_2O filters (40)	-0.523	7.34	0.74	1.85	0.19	-	0.2

*Uncorrected for solution absorbance and iR drop; unstirred solution.
†NR = $i_{peak} - I_{steady\text{-}state} / I_{peak}$

listed are the actual concentrations of the ions, taking into account the K(dissoc) of I_3^- in acetonitrile. At 1.0M TBAI, the solution resistance was approximately equal to that of the other solutions with 1.0M $TBABF_4$ supporting electrolyte, therefore no $TBABF_4$ was added.

At constant He-Ne intensity, all EPC parameters were improved with increasing I^- concentration. Cell #4 represents the best cell measured to date under intensity or hole-limited conditions. That is, concentration polarization at n-GaAs does not limit the cell output. This is shown by the fact that the normalized ratio (NR) which is defined by Cahen et al. (20) as the peak current density minus the steady-state current density, which represents the output loss of the cell with time, divided by peak current density,

$$NR = \frac{(i_p - i_{ss})}{i_p} \qquad (7)$$

where NR = 0 means no loss, and NR = 1 means total loss, or, no steady-state output. It should be emphasized that these are half cell measurements and represent losses at the semiconductor only. When cell #4 is run as a two electrode "solar cell," polarization losses at the Pt cathode limit the cell output indicating that the I_3^- concentration must be increased.

At higher light intensities, represented here by cell #4 run at 40 mW/cm^2 Xe, the half cell again is concentration limited as shown by the increase in NR. The large decrease in fill factor and power efficiency (η) reflects the substantially increased iR drop in the cell and light losses due to solution absorbance over the entire visible spectrum. Both are expected to be minimized in a thin cell format. The concentration of I^- can be increased to its saturation limit of 1.1M.

H. Counter Electrode Materials

Hodes et al. (21) has recently discussed the importance of the counter electrode in the EPC solar cell. In short, the counter electrode must be capable of supporting high steady-state current densities (for unstirred or nonflow format) with a minimum of overpotential. Maximum power efficiency at the semiconductor electrode determined from half cell current-voltage plots may never be realized in an actual cell. Therefore, it is equally important to study the counter electrode reaction and to compromise the relative concentrations of the [ox]/[red] couple in solution as well as the counter electrode size and material to realize the highest possible efficiency of the whole cell.

The following electrode materials have been evaluated in the PC, AN, DMF, MeOH and aqueous iodide/iodine electrolytes: shiny platinum (PtS), Pt-black (PtB), carbon cloth (CC), Teflon-bonded graphite (TBG),

indium-tin oxide coated glass (ITO) and tin oxide coated glass (TO). Electrodes were prepared with 1 cm^2 exposed geometric area, and studied in a 3-electrode cell of 4 ml capacity with a large area Pt cylinder as the counter electrode and a Pt wire in a Luggin capillary, filled with the same redox electrolyte as the bulk solution, as the reference electrode. Current-voltage curves under scanning (20 mV/sec) and steady-state conditions were obtained. Reduction currents at each electrode recorded at -0.06V polarization from equilibrium are compared in Table 13 for each electrode in electrolytes 0.01M in I_2 and 0.1M in I^-. In addition, Figure 19 shows the steady-state results for two acetonitrile solutions each containing 1M $TBABF_4$ as the supporting electrolyte, and the indicated formal concentrations of I_2 and TBAI.

The results for reduction of I_3^- on the ITO and TO glass electrodes which are typical for all the solvents studied here explain the large shift toward positive potentials when our thin cell (Section II.B) was run in the solar cell mode, i.e.,

$$n\text{-GaAs}/PC,\ I_2/I^-/ITO$$

thus reducing i_{sc} and the power efficiency (see Figure 20).

Obviously the optically transparent electrodes are not the counter electrodes of choice for use with the I_3^-/I^- redox couple. In general, best results were obtained for high surface area electrodes such as PtB and TBG. TBG is frequently employed as a high rate current collector in nonaqueous battery systems. The large difference between scanning and steady-state currents is a result of concentration polarization, possibly aggravated by precipitation of iodide salts on the electrode surfaces. It is noteworthy that H_2O outperforms the nonaqueous solvents due primarily to its higher conductivity.

This study is mainly for comparative purposes, rather than for EPC design. Clearly, more concentrated redox solutions are required to carry the currents of >15 mA/cm^2 encountered in solar cells. Furthermore, the physical size and conformation of the counter electrode must be carefully matched to the n-GaAs output capability under unstirred steady-state conditions and AM1 light intensity in order to realize the highest cell efficiency.

TABLE 13

RATES OF ELECTROCHEMICAL I_3^- REDUCTION AS A FUNCTION OF ELECTRODE MATERIAL AND SOLVENT. SOLUTIONS CONTAINED 0.01M I_2, 0.01M TETRABUTYLAMMONIUM IODIDE, 1M TETRABUTYLAMMONIUM TETRAFLUOROBORATE. NUMBERS ARE CURRENTS IN mA/cm^2 RECORDED DURING A VOLTAGE SCAN OF 20 mV/sec AND AT STEADY-STATE, RESPECTIVELY.

	Carbon Cloth	Smooth Pt	Teflon Bonded Carbon	Pt Black	ITO (NESATRON) Glass	TO (NESA) Glass
Acetonitrile	0.4/0.13	0.95/0.11	0.33/0.20	8.6/0.95	0.004/0.002	$6x10^{-4}/2x10^{-4}$
DMF	0.03/0.01	0.25/0.2	0.35/0.27	2.4/0.59	$<10^{-4}/<10^{-4}$	$<10^{-4}/<10^{-4}$
MeOH	0.2/0.11	1.45/0.83	0.85/0.56	8.0/0.94	$7x10^{-4}/3x10^{-4}$	0.001/0.0008
H_2O	5.85/1.45	6.6/1.75	12.5/2.35	9.5/1.75	$<10^{-4}/<10^{-4}$	$<10^{-4}/<10^{-4}$

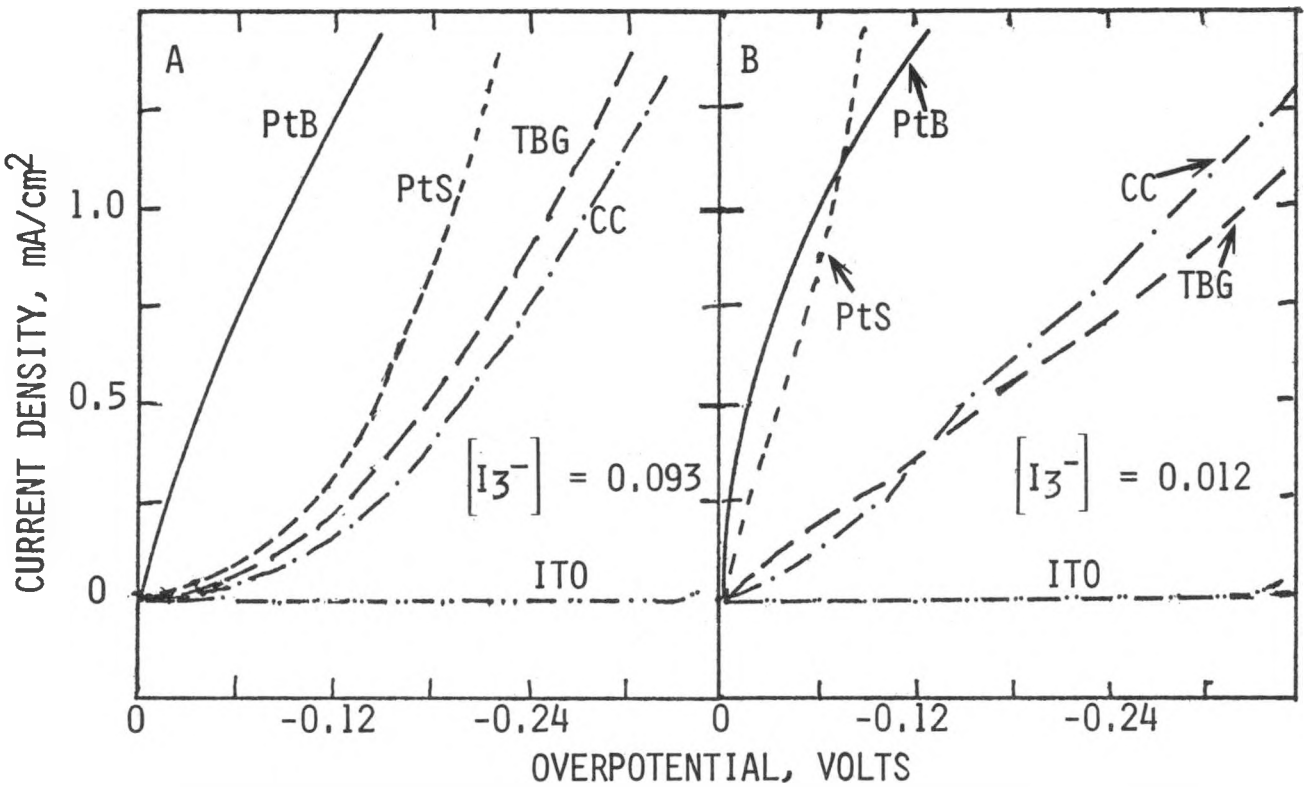

Fig. 19: Current per unit geometric area for reduction of I_3^- in AN on various electrode materials. Formal concentrations: A, 0.01 I_2/0.11 TBAI; B, 0.1 I_2/0.1 TBAI. Supporting electrolyte 1M $TBABF_4$.

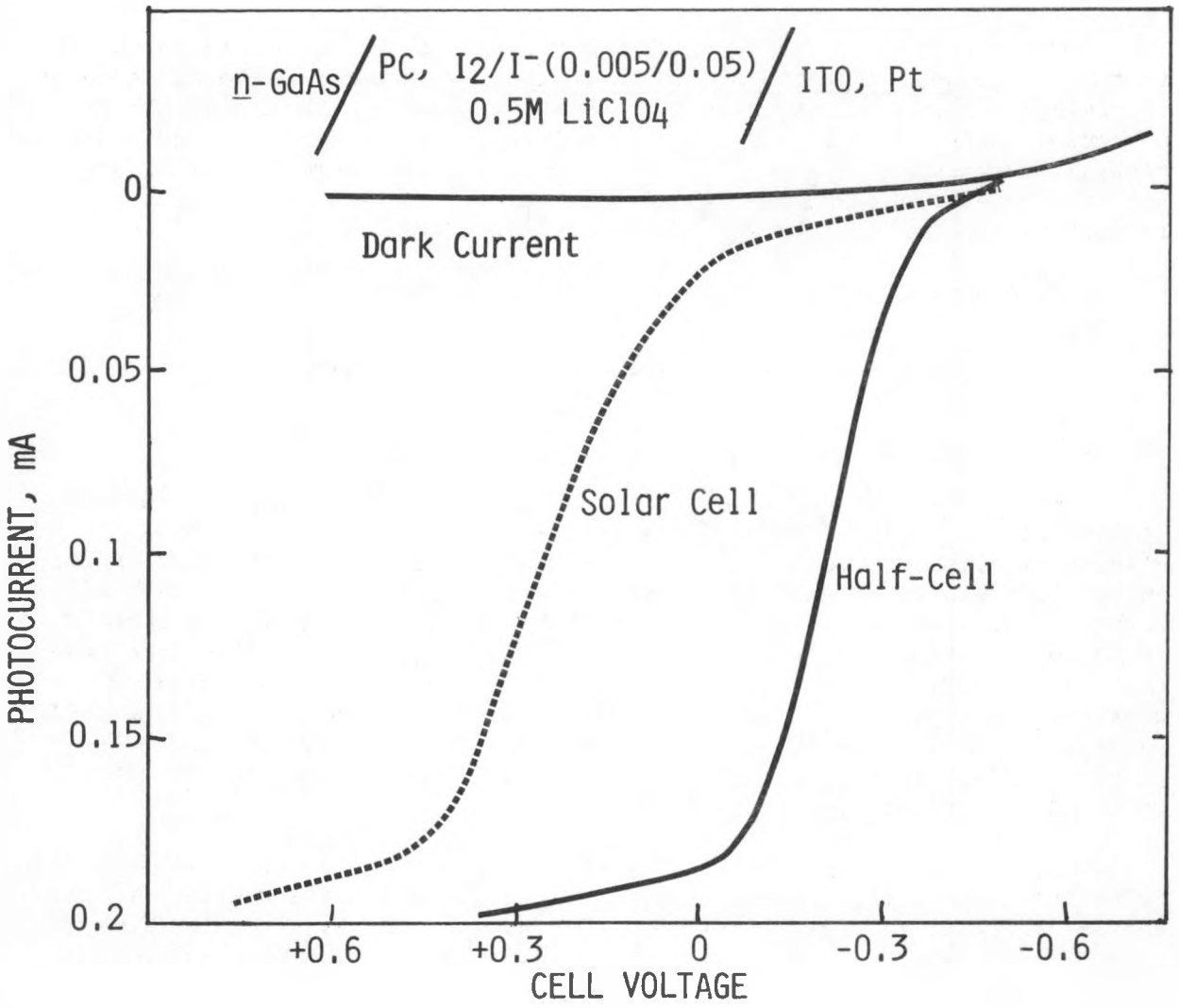

Fig. 20: Thin cell photocurrent vs. voltage curve at the same light intensity but run in half-cell and solar cell modes, showing effect of polarization of the ITO electrode on i_{SC} and cell output. Cell thickness, 0.38 mm.

IV. REDOX ELECTROLYTE PREPARATION BY ANODIC DISSOLUTION OF METALS IN PROPYLENE CARBONATE

The preparation of truly anhydrous metal ion redox couple solutions in aprotic organic solvents can be a difficult task due to several factors: (a) bulky covalent anions which help to render the metal salts stable in nonaqueous solvents also result in tenacious retention of waters of hydration; (b) some oxidation states which are stable in nonaqueous media are not available in a convenient solid form because of instability with respect to air, or water, or to disproportionation.

Anodic dissolution of Cr and Cu metal in the cell

$$Li/PC,\ 0.5M\ LiClO_4//PC,\ 0.5M\ LiClO_4/Metal$$

has been investigated under galvanostatic conditions.

• Chromium. In the case of chromium, only the Cr(III) is formed (and Li plated on the Li cathode) when the voltage of the above cell is allowed to climb to about 4.2V but no higher. The concentration of chromium in solution was determined spectrophotometrically by the diphenylcarbazide method (22,23) and related to the total charge passed. This corresponded to three electrons per Cr ion. A cyclic voltammogram on Pt with an anodic-first sweep indicated no oxidation reaction corresponding to $Cr^{+2} \rightarrow Cr^{+3} + e$ confirming that all Cr(II), if initially formed, had been oxidized to Cr(III) under the anodizing conditions used. A sweep in the cathodic direction produced Cr^{+2}. Therefore, it should be possible to prepare Cr^{+2} from Cr^{+3} by controlled potential electrolysis.

V. Gutman et al.(24) have reported three, one electron polarographic reduction steps for $Cr(ClO_4)_3 \cdot 6H_2O$ in PC. We have no evidence to support the existence of the Cr(I) under dry conditions. In PC, concentrations of Cr^{+3} became limited to $<5 \times 10^{-3}M$ by Cr electrode passivation, presumably due to precipitation of the anhydrous perchlorate salt.

• Copper. In 0.5M $LiClO_4$ solutions in PC, several anodic dissolution experiments were run. A Li electrode wrapped in microporous polypropylene (Celgard, Celanese Corp.) was employed as the counter electrode. If the potential was kept below 3.7V (by controlling the current density), a blue-green solution is formed, and at long electrolysis times, a dark blue-green precipitate of $CuClO_4$ forms. The solution was analyzed for total dissolved Cu by the neocuproin method (25). On exposure to air, the solution becomes yellow due to air oxidation to Cu(II). In one cell where the potential was allowed to go higher than 3.7V, a yellowish-green solution resulted probably due to a mixture of Cu(I) and Cu(II). As shown in Table 14, dissolutions were close to quantitative, with the exception of some precipitate.

TABLE 14

RESULTS OF ELECTROCHEMICAL DISSOLUTION OF Cu IN ANHYDROUS, PROPYLENE CARBONATE. DISSOLUTIONS CARRIED OUT GALVANOSTATICALLY AT 1 mA/cm^2. $[Cu^{++}]$, $[Cu^{+}]$ CALC. ARE VALUES ASSUMING ALL DISSOLVED Cu IN GIVEN OXIDATION STATE.

Supporting Electrolyte	Average V(Cu) vs. Li^+/Li	Time Run (hr)	Final Solution Color	Precipitate Color	$[Cu]_{total}$	$[Cu^{++}]$ Calc	$[Cu^{+}]$ Calc
0.5M $LiClO_4$	3.69	24	blue	blue-green	0.0032	0.0018	0.0036
0.5M $LiClO_4$	3.52	72	blue	blue-green	0.0063	0.005	0.01
0.5M $LiClO_4$	3.55	96	blue	blue-green	0.008	0.007	0.014
0.5M $LiAsF_6$	3.54	142,	yellow	copper-colored	0.012	0.01	0.02

When $LiAsF_6$ was used as the supporting electrolyte, a yellow solution resulted and Cu precipitated on all surfaces of the cell. We believe this to be due to a disproportionation reaction similar to that in H_2O.

$$2Cu^{+} + 2e \rightarrow Cu^{+2} + Cu^{\circ}\downarrow \qquad (8)$$

This is borne out by the Cu(II) concentration found in solution and the electron charge passed in the cell. Again the Cu(II) is yellow in color. Apparently ClO_4^- stabilizes Cu(I) in PC with respect to the disproportionation reaction, but it also causes $CuClO_4$ to precipitate at a concentration less than that required for effective EPC operation.

V. SEMICONDUCTOR ELECTRODE FABRICATION

A. Screen Printing

It is well recognized that a practical EPC must utilize both inexpensive and conservative quantities of semiconductor materials. EPCs utilizing expensive crystals operating at high light intensities would seem to be ruled out due to the current-limiting processes associated with the diffusion of active species in the electrolyte.

The application of thick film screen printing technology to fabricating active electrode elements for solar cells has been recently demonstrated by Nakayama et al. (26). These authors printed both CdS and CdTe films in fabricating the cell of 8.1% AM1 efficiency. Hodes et al. have also reported recently on CdSe/CdTe solid solution photoelectrodes formed by sintering inks on pastes with an organic base (27).

Precision screen printing of electronic devices is an established technology, although it has been generally a tool for the production of passive circuit elements. There should be no difficulty in eventual commercial production of screen printed photoelectrodes at low cost. There is also the possibility of printing complicated electrode structures, such as interlocking fingers of p- and n-doped semiconductors.

For laboratory investigations we have constructed a small, manually operated screen printing device, based on commercially available 5" x 7" cast aluminum framer fitted with 200 mesh stainless steel screens. Its important feature is that the distance between the screen and the substrate is controlled with four adjustment screws and can be measured with a probe micrometer. This gap, the "snap-off distance," is an important variable in the thickness of the deposited film. In the course of a printing stroke, the squeegee moves over the screen, deforming it so that it touches the substrate as it squeezes ink through the mesh. Behind the squeegee, the screen snaps back from the substrate; the faster it snaps back, the more ink is left on the substrate.

Another parameter controlling film thickness is ink viscosity. A more viscous ink will tend to stay with the screen as it snaps back, leaving a thinner film. The inks are produced by combining a finely ground mixture of semiconductor and flux with an organic binder and an appropriate solvent. The ratio of solvent to binder is the main factor in ink viscosity; our initial printing experiments have used butyl cellosolve and ethyl cellulose in ratios between 95% and 60%/40%.

1. CdS. Sintered layers of CdS were prepared in an attempt to duplicate the method of Sihvonen, Parker and Boyd (28). A CdS film was prepared on a conductive glass substrate and was used as the photoelectrode in a CdS ($CdCl_2$ doped)/Na_2S(1M), S, NaOH(sat)/Pt electrochemical cell. Using this crude film, an efficiency of 0.28% was achieved at 10 mW/cm^2.

2. CdSe. A number of printing variables have been explored in the fabrication of CdSe electrodes. Substrates have included NESATRON glass, molybdenum, aluminum, etched stainless steel and sputtered films of Ni and Ti on glass supports. Oxidation of Ni and Al substrates during sintering eliminated them from consideration. Films were evaluated in a two electrode EPC configuration with an aqueous polysulfide electrolyte (1M Na_2S, 1M S, 1M NaOH) and a Pt counter electrode. Illumination was as described in Table 15.

Ink composition and sintering conditions had marked effects on electrode performance. A series of CdSe inks were prepared, all 10:3 molar mixtures of CdSe:$CdCl_2$. Two parameters were varied; half had 8×10^{-4} mol % $CuCl_2$ as an activator and the powder mixtures were presintered at 550°C in flowing argon for 0, 30 and 60 minutes.

The powders sintered into lumps with hard surfaces, and the inks made from them produced lower quality films than those without presintering. Qualitative measurements of resistance and photoconductivity gain indicated that the $CuCl_2$ activator increased photosensitivity and dark resistance and that sintering temperatures of 600°C increased sensitivity compared to 550°C sintering.

Three groups of activated, non-presintered CdSe electrodes were prepared on NESATRON glass with sintering times of 5, 20, and 60 minutes at 600°C. As shown by the data in Table 15, sintering times of 20 and 60 minutes produced films with similar performance, but better than those sintered for 5 minutes. No significant differences were noted between front and back illumination of the electrodes. Efficiencies for the better samples were on the order of 0.10% at 80 mW/cm^2 filtered source illumination, although it should be kept in mind that the cell configuration was chosen for ease of use in the comparison of relative performance, not optimal performance.

The etched molybdenum substrates have proved to be slightly superior to NESATRON, both in open circuit photovoltage and in photocurrent. Figure 21 shows typical I-V curves for CdSe on Mo in aqueous polysulfide. A final etching treatment with chromic acid also improves film performance.

Several modifications of the ink composition were made in an attempt to enhance film performance. In each case, sintering sequences were determined by thermogravimetric analysis of volatilization or combustion of ink components. In one series of experiments, the binder was changed

TABLE 15

CdSe SINTERED ELECTRODES IN 1M NaOH, Na_2S, S vs. Pt COUNTER ELECTRODE. ILLUMINATED AT 80 mW/cm^2 WITH A XENON LAMP FILTERED THROUGH PYREX GLASS AND DISTILLED WATER. ELECTRODE SURFACE AREAS ARE APPROXIMATELY 1 cm^2.

Substrate	Sintering Time (min. at 600°C)	Sample	Front Illumination V_{oc} (volts)	Front Illumination i_{sc} (mA)	Back Illumination V_{oc}	Back Illumination i_{sc}
NESATRON	5	1	-0.44	0.8-1.0		
		2	-0.44	0.8-1.0		
NESATRON	20	1	-0.49	∿0.85		
		2	-0.51	0.8-1.0		
Etched Steel	20	1	-0.21	0.15		
		2	-0.04	0.03		
NESATRON	60	1	-0.50	0.8-1.0	-0.39	0.8-1.0
		2	-0.49	0.8-1.0	-0.47	0.8-1.0
Molybdenum	20	1	-0.49	0.93		
		2	-0.49	1.08		
Molybdenum (with post-sinter etch in chromic acid)	20	1	-0.62	1.34		
		2	-0.58	1.56		

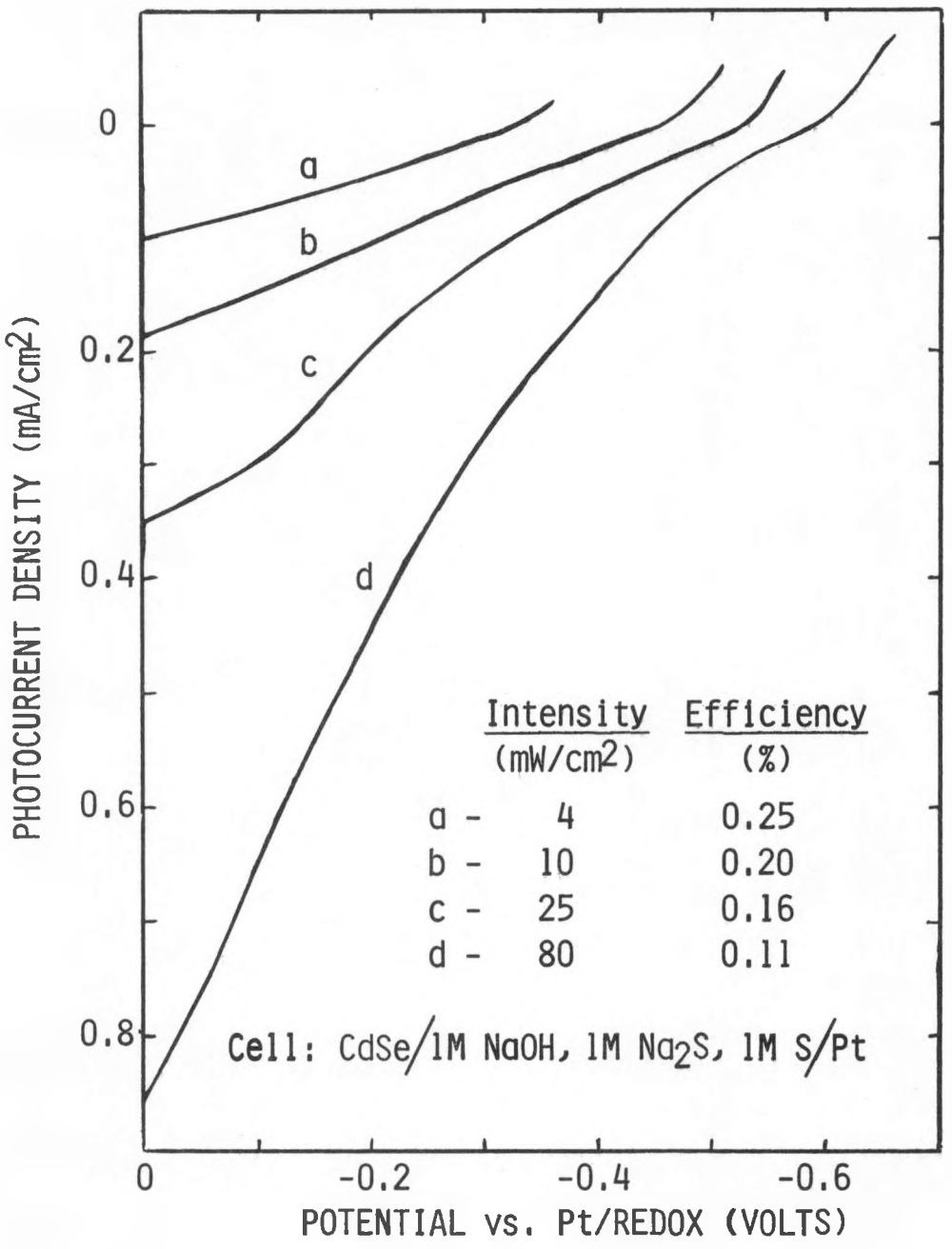

Fig. 21: Photocurrent-voltage curves at several illumination intensities using a pyrex and H_2O filtered Xe arc attenuated by neutral density filters. CdSe film printed on Mo substrate sintered 20 min at 600°C in flowing Ar. $CdCl_2$ flux; $CuCl_2$ activator; chromic acid etch.

to a composition which would evaporate below 350°C, rather than requiring combustion. This permits the use of an inert atmosphere at all times, thus eliminating the problem of oxidation of CdSe. The films produced entirely under argon are matte black, rather than the gray color of films which undergo a binder burnoff. The binders tried so far are based on 1,6-hexanediol, which has a melting point of 41°C and a boiling point of 250°C.

Changing the flux from $CdCl_2$ to Se produced some films of small photoresponse and generally poor adhesion. There is some hope for Se as a flux. On one sputtered Ti substrate, there were patches of what appeared to be a glassy, adherent film, underneath an otherwise poor deposit. These patches also had a small photoresponse, however.

3. CdTe. Preliminary results indicate that CdTe is considerably less stable to sintering than CdS. Initial experiments involving the preparation of CdTe layers on steel and NESATRON substrates have resulted in films of poor adhesion and very small photoresponse. Annealing of CdTe in air at 500-600°C, necessary to vaporize the $CdCl_2$ flux, ultimately results in contamination of the final layer with TeO_2. Similar oxidative decomposition of CdS is not noted under the same reaction conditions. For the reaction

$$\frac{3}{2} O_2 + CdX \rightarrow CdO + XO_2 \qquad (9)$$

ΔG = -92 kcal/mole for CdS and -94.6 kcal/mole for CdTe. It is possible, however, that the initial rate determining process is

$$\frac{1}{2} O_2 + CdX \rightarrow CdO + X \qquad (10)$$

for which there is a great difference in ΔG: -20.2 kcal/mole for CdS and -30.0 kcal/mole for CdTe.

B. Plating Cd Chalcogenide Electrodes

The investigation of cadmium chalcogenide thin film formation has been extended from screen printing to electrodeposition and chemical bath deposition techniques.

1. Electrodeposition. Thin films of cadmium selenide have been electrodeposited by the method of Hodes, Manassen and Cahen (29) from solutions of 1M H_2SO_4, 0.4 mM SeO_2, and 0.1M $CdSO_4$ using a cadmium anode and a titanium cathode substrate. As with the electrodeposition of cadmium telluride (30), the process is a codeposition of separate metals, limited to the rate of chalcogenide deposition and sensitive to stirring rates. The deposition occurs spontaneously when the two electrodes are externally shorted. Cathode potential was -0.66V vs. SCE at 2 mA/cm^2. Average film

thickness was determined by weight to be approximately 1.5 microns prior to heat treatment for 4 hours at 500°C, followed by a 15 second etch in 10M HCl at 25°C. Depositions on amorphous materials, such as sputtered titanium or transparent In_2O_3 on glass, were richer in selenium content, passivating more quickly during plating and adhered poorly. Parameters of heat treatment, etch and film thickness will be optimized. Preliminary results are shown in Table 16.

2. Chemical Bath Deposition. Cadmium selenide films were deposited by the method of Kainthla, Pandya and Chopra (31) in an aqueous solution of 0.05M cadmium acetate, 0.05M sodium selenosulfate and 2.1M ammonium hydroxide. Cadmium (II) forms a complex with four ammonia molecules to give $Cd(NH_3)_4^{2+}$, while there is an equilibrium amount of selenium (II) available by reaction of the selenosulfate with base:

$$Na_2SeSO_3 + OH^- \rightleftarrows Na_2SO_4 + HSe^- \quad (11)$$

$$HSe^- + OH^- \rightleftarrows H_2O + Se^{2-} \quad (12)$$

At bath temperatures above 70°C, there are sufficient selenium (II) ions available to allow the formation of cadmium selenide.

We have determined that heat treatment and acid etch are essential to good electrode characteristics; our present experiments are designed to optimize these factors. Furthermore, it seems that copper (II) added to the bath as an activator does not enhance film performance, which was surprising considering its effects in cadmium chalcogenide films produced by other methods.

Preliminary results of these chemically deposited films are summarized in Table 17.

TABLE 16. PHOTOELECTROCHEMICAL RESPONSE OF ELECTRODEPOSITED CdSe FILMS†

Plate No.	Prior to Heat Treatment		After 4 hr, 500°C		After Etch	
	Voc (volts)	isc (mA/cm2)	Voc (volts)	isc (mA/cm2)	Voc (volts)	isc (mA/cm2)
1-14 (Ti)	-0.25	+0.44	-0.51	+1.30	-0.60	+2.51
2-14B(Ti)	-0.24	+0.67	-0.50	+2.25	-0.51	+4.20
3-18 (Ti)	-0.22	+0.47	-	-	-0.45	+3.00
4(In_2O_3)	-0.13	+0.13	-0.22	+0.14	-	-
5(sputtered Ti)	-0.06	+0.01	-	-	-	-

*pH = 0.5, temperature 27°C.

†Photoelectrochemical measurements made with Xe arc lamp. A total intensity of 80 mW/cm2 empinges on the cell. Thickness of 1M Na_2S, 1M NaOH, 1M S electrolyte is 1 cm.

TABLE 17. ELECTROLESS DEPOSITED CdSe FILMS ON TITANIUM†

Film No.	Cu^{+2}/Cd^{+2} Ratio in Bath	Prior to Heat Treatment		After 1 hr, 500°C		After 3 sec Etch (10M HCl)	
		Voc (volts)	isc (mA/cm2)	Voc (volts)	isc (mA/cm2)	Voc (volts)	isc (mA/cm2)
1	no Cu	0.17	-0.1	-0.38	+1.7	-0.43	+2.7
2	no Cu	-0.10	+0.1	-0.40	+2.2	-0.43	+3.0
3	$1:10^4$	-0.08	+0.1	-0.23	+1.1	-0.40	+1.9
4	$1:10^4$	+0.06	-0.1	-0.20	+1.0	-0.18	+1.3
5	$1:10^3$	-0.07	+0.1	-0.27	+1.0	-0.40	+1.4
6	$1:10^3$	+0.18	-0.3	-0.10	+0.5	-0.05*	+0.4
7	$1:10^2$	-0.20	+0.2	-0.42	+1.2	-0.32	+1.0
8	$1:10^2$	-0.15	+0.1	-0.15	+0.5	-0.39	+1.3

*5 sec etch.

†Photoelectrochemical measurements made with Xe arc lamp. A total intensity of 80 mW/cm2 empinges on the cell. Thickness of 1M Na_2S, 1M NaOH, 1M S electrolyte is 1 cm.

VI. SUMMARY AND CONCLUSIONS

This initial twelve months of research on nonaqueous EPCs has focused on n-GaAs as a model photoelectrode in several nonaqueous solvents. Measurements on a variety of redox couples in PC electrolytes have indicated several limiting factors in these devices. Photovoltages were somewhat sensitive to the position of V_{redox}, but were limited to $<\sim 0.7V$ by decomposition of the semiconductor. Redox couples which lie too positive of V_{fb}, are likely to act as etchants; indeed, Br_2 is a common etchant for GaAs. Furthermore, the redox couples explored in this work appear not to have adsorptive effects on the onset of photocurrent, which occurred at a common potential of $\sim -0.3V$ vs. SCE in all the PC-based systems. In aqueous solutions, negative shifts of V_{fb} due to adsorption of redox species can provide an increased range of photovoltages, e.g., n-GaAs/aqueous Se_2^{-2}, Se^{-2} devices. Although more positive-lying redox couples can stabilize GaAs in PC than in water (e.g., ferrocene, I_3^-), photovoltages are no greater in the nonaqueous systems due to the lack of such adsorptive effects. Nevertheless, nonaqueous systems do have the advantage of allowing a wider variety of stabilizing redox couples than aqueous solutions. It is our hope that less noxious electrolytes than Se_2^{-2}/Se^{-2} can be developed in nonaqueous systems.

Another potential difficulty with nonaqueous EPCs is the problem of mass transport. In several studies summarized in this report, it has been shown that efficiencies degrade seriously with increasing light intensity in nonaqueous electrolytes. Counter electrode materials also show inferior kinetics to I_3^- reduction, for example, in nonaqueous compared to aqueous electrolytes. If high photovoltages can be achieved in nonaqueous systems because of their increased stabilizing range, then high efficiencies can be achieved with reduced currents, i.e., P_{max} = 10 mA/cm^2 x 1V, rather than P_{max} = 20 mA/cm^2 x 0.5V. However, adsorbing redox couples in nonaqueous electrolytes or other semiconductor surface modifications will be necessary to achieve such high voltages.

To minimize mass transport polarization in nonaqueous EPCs, highly conductive electrolytes such as CH_3CN or DMF are desirable. Although conductivities of the best nonaqueous systems are still considerably lower than aqueous electrolytes, polarization losses due to ohmic drop might still be acceptable with an optimized cell design. A related problem is the solubilities of redox species attainable in nonaqueous solvents. The I_3^- system is one of the few economical species with a solubility in nonaqueous solvents high enough to maintain currents required in solar cells. However, large optical density throughout the visible spectrum limits its utility in a front illuminated cell. Other sample couples like Cu^{+2}/Cu^+, Sn^{+4}/Sn^{+2} and $Fe(CN)_6^{-3}/Fe(CN)_6^{-4}$ would be preferable due to their lighter color, if their solubilities can be made large.

Results on printed, chemically deposited, and electrodeposited II-VI films point out the interesting possibilities for providing very economical electrode structures for EPCs. Even for some of the rather crude films prepared in our preliminary studies, the liquid junction allows the measurement of a photovoltaic response. Processing of the same films into all solid-state devices would have been impossible.

VII. REFERENCES

1. A. B. Ellis, S. W. Kaiser, J. M. Bolts and M. S. Wrighton, J. Am. Chem. Soc., 99, 2839 (1977).

2. S. M. Sze, Physics of Semiconductor Devices (New York: Wiley-Interscience, 1969), p. 363 ff.

3. B. Parkinson, A. Heller and B. Miller, Appl. Phys. Letters, 33, 521 (1978).

4. W. D. Johnson, H. I. Leamy, B. A. Parkinson, A. Heller and B. Miller, J. Electrochem. Soc., 127, 90 (1980).

5. H. Hovel, Solar Cells: Semiconductors and Semimetals, R. K. Willardson and A. C. Beer, eds. (New York: Academic Press, 1975), Vol. 11.

6. C. H. Seager and D. S. Ginley, Appl. Phys. Letters, 34, 337 (1979).

7. A. J. Bard, A. B. Bocarsly, F. F. Fan, E. G. Walton and M. S. Wrighton, J. Am. Chem. Soc., 102, 3671 (1980).

8. R. H. Wilson, J. Appl. Phys., 48, 4292 (1977).

9. D. Sawyer, Experimental Electrochemistry for Chemists (New York: John Wiley and Sons, 1975).

10. J. O. Besenhard and G. Eichinger, J. Electroanal. Chem., 68, 1 (1976).

11. R. Parsons, Handbook of Electrochemical Constants (London: Butterworths, 1959).

12. N. Matsuura, K. Umimoto and Z. Takeuchi, Bull. Chem. Soc. Japan, 47, 813 (1974).

13. I. M. Kolthoff and F. G. Thomas, J. Phys. Chem., 69, 3049 (1965).

14. P. A. Kohl and A. J. Bard, J. Electrochem. Soc., 126, 603 (1979).

15. R. T. Iwamoto, Anal. Chem., 31, 955 (1959).

16. I. Shiota, K. Motoya, T. Ohmi, N. Miyamoto and J. Nishizawa, J. Electrochem. Soc., 124, 155 (1977).

17. B. A. Parkinson, A. Heller and B. Miller, J. Electrochem. Soc., 126, 954 (1979).

18. A. I. Popov and D. H. Geske, J. Am. Chem. Soc., 80, 1340 (1958).

19. D. Tench and L. Warren, Second Quarterly Progress Report, SERI Subcontract No. XP-9-8002-1, October 1979.

20. D. Lando, J. Manassen, G. Hodes and D. Cahen, J. Am. Chem. Soc., 101, 3969 (1979).

21. G. Hodes and J. Manassen, J. Electrochem. Soc., 127, 544 (1980).

22. T. L. Allen, Anal. Chem., 30, 447-450 (1958).

23. B. E. Saltzman, Anal. Chem., 24, 1016-1020 (1952).

24. V. Gutman, M. Kogelnig and M. Michlmayr, Monatsh., 99, 707 (1968).

25. A. R. Gahler, Anal. Chem., 26, 577 (1954).

26. N. Nakayama, H. Matsumoto, Y. Yamaguchi, S. Ikegami and Y. Hioki, Japan J. Appl. Phys., 15, 2281 (1976).

27. G. Hodes, D. Lando, J. Manassen and D. Cahen, Fall Meeting of The Electrochemical Society, Los Angeles, 1979. Abstract 699 RNP.

28. S. Chen and Z. Kiss, Second Electrochemical Photovoltaic Cell Contractors' Meeting, Arlington, VA, January 23 and 24, 1980.

29. G. Hodes, J. Manassen and D. Cahen, Nature, 261, 403 (1986).

30. M. P. R. Panicker, M. Knaster and F. A. Kroger, J. Electrochem. Soc., 125, 566 (1978).

31. R. C. Kainthla, D. K. Pandya and K. L. Chopra, J. Electrochem. Soc., 127, 277 (1980).

☆U.S. GOVERNMENT PRINTING OFFICE: 1981-740-145 2299